

Bayesian nonparametric models for zero-inflated count-compositional data using ensembles of regression trees

André F. B. Menezes¹, Andrew C. Parnell², and Keefe Murphy¹

¹Hamilton Institute and Department of Mathematics and Statistics, Maynooth University

²School of Mathematics and Statistics, Insight Centre for Data Analytics, University College Dublin, Ireland

Abstract

Count-compositional data arise in many different fields, including high-throughput microbiome sequencing and palynology experiments, where a common, important goal is to understand how covariates relate to the observed compositions. Existing methods often fail to simultaneously address key challenges inherent in such data, namely: overdispersion, an excess of zeros, cross-sample heterogeneity, and nonlinear covariate effects. To address these concerns, we propose novel Bayesian models based on ensembles of regression trees. Specifically, we leverage the recently introduced zero-and- N -inflated multinomial distribution and assign independent nonparametric Bayesian additive regression tree (BART) priors to both the compositional and structural zero probability components of our model, to flexibly capture covariate effects. We further extend this by adding latent random effects to capture overdispersion and more general dependence structures among the categories. We develop an efficient inferential algorithm combining recent data augmentation schemes with established BART sampling routines. We evaluate our proposed models in simulation studies and illustrate their applicability with two case studies in microbiome and palaeoclimate modelling.

Keywords: Bayesian additive regression trees, Bayesian nonparametrics, count-compositional data, latent random effects, overdispersion, zero-inflation.

1 Introduction

Count-compositional data arise in many scientific fields where multivariate counts are constrained by a fixed or random total, representing the frequencies of outcomes across several mutually exclusive categories. We are particularly motivated by two biological case studies where the counts are sparse: a high-throughput microbiome sequencing experiment, where the counts correspond to the observed composition of different microbial taxa in the human gut (Wu et al., 2011), and a palynology study, where the counts are the frequency with which pollen species appear in sediment cores (Haslett et al., 2006). A common goal in such studies is to understand how sample-specific covariates are associated with the observed compositions. In the first study, the covariates relate to the dietary intake of individuals. In the second study, which relates to palaeoclimate research, the covariates are proxies for the climate in the locations of the sediment cores.

The data from such studies often present several key challenges. They are typically high-dimensional, involving a large number of categories and/or covariates and, relative to the multinomial sampling distribution, exhibit an excess of zeros, more complex dependence structures, and overdispersion. Simple extensions, such as the Dirichlet-multinomial (DM) model (Mosimann, 1962), are unable to adequately accommodate all of these characteristics. Another challenge is overcoming the overly restrictive assumption, often made in analyses of such data, that the covariates are linearly related to the observed compositions. This article introduces two models based on flexible Bayesian nonparametric priors that simultaneously address these challenges. We begin by reviewing existing methods and highlighting their limitations which motivated our development of novel modelling strategies. We then summarise our main contributions.

1.1 Literature review

Many methods have been proposed to account for the aforementioned features of count-compositional data, mainly through extensions of the multinomial and DM distributions. [Chen and Li \(2013\)](#) and [Xia et al. \(2013\)](#) proposed sparse group penalty methods for variable selection using log-linear DM and logistic normal multinomial regression models, respectively. As another means of performing variable selection, [Wadsworth \(2017\)](#) proposed a Bayesian treatment of the log-linear DM regression model with spike-and-slab priors. To deal with many taxa in microbiome studies, [Grantham et al. \(2020\)](#) proposed a multinomial logistic regression model with both fixed and random effects and a common factor analysis hyperprior. [Ren et al. \(2017\)](#) defined a dependent Dirichlet process as a prior for the multinomial probabilities and introduced dependence through the shrinkage-inducing factor analysis hyperprior of [Bhattacharya and Dunson \(2011\)](#). [Ren et al. \(2020\)](#) presents a further extension to accommodate linear covariate effects.

A clear limitation of the above methodologies is that they do not explicitly accommodate an excess of zeros, which can arise due to sampling variability or structural absence ([Blasco-Moreno et al., 2019](#)). This has motivated the development of count-compositional models with components to explicitly capture structural zeros. [Zeng et al. \(2023\)](#) proposed a zero-inflated logistic normal multinomial model by parametrising the individual-level multinomial probabilities with a mass at zero and a probabilistic principal component analysis structure. [Koslovsky \(2023\)](#) proposed the zero-inflated Dirichlet-multinomial (ZIDM) model, by modifying the Dirichlet prior formulation via normalised independent gamma random variables augmented with point masses at zero, and extended this framework with linear functional forms to link covariates to the compositional and structural zero probabilities with further spike-and-slab priors for variable selection. The zero-inflated generalised Dirichlet-multinomial regression model of [Tang and Chen \(2019\)](#), which predates the ZIDM model but omits the spike-and-slab priors, relaxes the restrictive assumption of negative dependence between categories that characterises the multinomial and DM distributions.

Despite these developments, another major limitation of existing methods is that the assumed relationship between covariates and the observed composition is expressed through parametric linear functional forms. While convenient, these assumptions can be restrictive and fail to capture nonlinear and complex covariate effects, leading to model misspecification. Methods developed within palaeoclimate research aiming to model the relationship between climate covariates on pollen compositions have adopted smooth functional forms. Notably, Gaussian Markov random field (GMRF) priors ([Rue and Held, 2005](#)) have been used extensively in this context (see, e.g., [Haslett et al., 2006](#); [Tipton et al., 2019](#)). [Haslett et al. \(2006\)](#) employed a log-linear DM model with GMRF priors defined on a two-dimensional climate space. Their model was extended by [Salter-Townshend and Haslett \(2012\)](#) to address zero-inflation through a nested hierarchical structure on the pollen species, which breaks the compositional nature of the data into conditionally independent univariate distributions. [Sweeney \(2012\)](#) further extended this by adding an additional climate covariate and employing the zero-and- N -inflated binomial distribution at the lowest hierarchical levels. Although GMRF priors induce smooth and flexible relationships between the pollen composition and climate covariates, they are computationally intensive when scaling beyond two dimensions. Approximations of the continuous GMRF based on discretisation such as those employed by [Salter-Townshend and Haslett \(2012\)](#) and [Sweeney \(2012\)](#) through the integrated nested Laplace approximation framework (INLA; [Rue et al., 2009](#)) are not immune to the curse of spatial dimensionality, and can also have high computational cost due to the large number of latent parameters to infer. [Tipton et al. \(2019\)](#) proposed a log-linear DM model with Gaussian process (GP) priors, though its broader applicability is limited as it only relates the pollen composition to a single climate covariate.

1.2 Our contributions

While existing methods address problem-specific aspects of count-compositional data motivated by their respective application contexts, they are not capable of addressing all aforementioned key challenges simultaneously, which limits their applicability. Our contribution fills this gap by developing Bayesian nonparametric models based on ensembles of regression trees that accommodate zero-inflation, overdispersion, and more complex

dependence structures, while flexibly capturing the effects of covariates.

Our approach builds on the zero-and- N -inflated multinomial (ZANIM) distribution which was introduced and characterised as a finite mixture distribution by [Menezes et al. \(2025\)](#). This probabilistic framework is designed to capture zero-inflation in count-compositional data and the related phenomenon of N -inflation, which refers to zeros co-occurring in all but one category. The ZANIM distribution has two sets of category-specific parameters, which describe the population-level count and structural zero probabilities. In this paper, our proposed models extend ZANIM by assigning independent nonparametric Bayesian additive regression trees (BART) priors ([Chipman et al., 2010](#); [Murray, 2021](#)) to both components, to flexibly incorporate covariate effects. Specifically, we employ the log-linear BART prior of [Murray \(2021\)](#) for the former and the probit-BART prior of [Chipman et al. \(2010\)](#) for the latter. Our framework thus accommodates nonlinear covariate effects and interactions at both levels without requiring pre-specification of the functional forms. We refer to this proposed extension as the ZANIM-BART model. Conceptually, this model extends the multinomial logistic BART model of [Murray \(2021\)](#) through the inclusion of category-specific BART priors for the structural zero probabilities. Doing so helps to mitigate bias in the estimated covariate effects on the compositional probabilities. To further accommodate overdispersion and capture more complex dependencies among the categories and across the samples, we also develop the ZANIM-LN-BART model, which incorporates log-linear multivariate Gaussian random effects on the compositional probabilities.

The success of BART in recovering unknown smooth functions and low-order interactions has been demonstrated empirically and theoretically by [Linero and Yang \(2018\)](#) and [Ročková and van der Pas \(2020\)](#). In addition, [Linero \(2017\)](#) established theoretical guarantees showing that BART approaches a GP prior as the number of trees tends to infinity. Supported by these results, we thus adopt BART as a nonparametric prior in our novel ZANIM-BART and ZANIM-LN-BART models to provide a flexible framework suitable for different count-compositional data analysis settings, such as our cases studies in microbiome and palynology experiments. The complexity of jointly adopting distinct ensembles of trees for both the compositional and structural zero probabilities, and doing so for each category, is mitigated through our novel adaptation of the data augmentation scheme developed for the ZANIM distribution ([Menezes et al., 2025](#)). This methodological contribution enables the development of an efficient Markov chain Monte Carlo (MCMC) algorithm with minor modifications of the established BART sampling routines of [Chipman et al. \(2010\)](#) and [Murray \(2021\)](#).

The rest of this paper is structured as follows. Section 2 reviews relevant background and describes the novel methodological aspects of our models, along with their associated inference schemes. Section 3 presents simulation studies which demonstrate that our proposed models accurately recover the compositional and structural zero probabilities in the presence of complex covariate effects, even when the data generating process is misspecified. We illustrate our models by analysing count-compositional data from microbiome and palynology experiments in Section 4. Specifically, Section 4.1 shows that our models notably outperform some competitors in an analysis of human gut microbiome data, while Section 4.2 shows that our models are able to uncover rich insights in an analysis of pollen-climate data. We conclude in Section 5 with a discussion. and defer many additional results to the Supplementary Material.

2 Methods

We assume that we observe a random sample of size n collected in the count matrix $\mathbf{Y} \in \mathbb{N}_0^{n \times d}$, where n denotes the number of samples and d the number of categories. Each row $\mathbf{Y}_i = (Y_{i1}, \dots, Y_{id})$ records the observed frequencies of the d mutually exclusive outcomes across N_i trials in sample i . Here, we consider the case where the total N_i is fixed. Formally, the random vector $\mathbf{Y}_i \in \mathbb{S}_{N_i}^d$ lies in the discrete simplex space constrained to an individual-specific total count N_i , where $\mathbb{S}_{N_i}^d = \{\mathbf{Y}_i \in (0, \dots, N_i)^d; \sum_{j=1}^d Y_{ij} = N_i\}$. The multinomial distribution is the natural probabilistic model for each observation, i.e., $\mathbf{Y}_i \sim \text{Multinomial}_d[N_i, \theta_1, \dots, \theta_d]$, where the parameter vector $\boldsymbol{\theta} = (\theta_1, \dots, \theta_d)$ corresponds to the population-level count (compositional) probabilities and lies on the continuous simplex space $\mathbb{S}_d = \{\boldsymbol{\theta} \in \mathbb{R}^d; \theta_j > 0, \sum_{j=1}^d \theta_j = 1\}$.

Estimation of $\boldsymbol{\theta}$ is crucial as it provides the information underlying the observed counts. Researchers often seek to estimate the association between these compositional probabilities and available covariates denoted by $\mathbf{x}_i = (x_{i1}, \dots, x_{ip})$. Typically, each θ_j is related to covariates through a suitable link function with a parametric linear functional form. Although convenient, this assumption imposes strong restrictions that limit the range of data generating processes that the model can capture. Moreover, count-compositional data sets with even a moderate number of categories d , such as those in our case studies (where $d = 28$ for both), are usually sparse and overdispersed, and exhibit more complex dependencies than the multinomial distribution allows.

To address these challenges, we introduce two nonparametric ensemble of regression trees models based on the zero-and- N -inflated multinomial (ZANIM) distribution. Section 2.1 reviews the ZANIM distribution and proposes an extension, which we refer to as the ZANIM-Lognormal (ZANIM-LN) distribution, to further capture overdispersion and complex dependences. We briefly review nonparametric BART priors, on which both of our models rely, in Section 2.2. Our novel models are then formulated in Section 2.3, where we assign BART priors on the compositional and structural zero probability parameters of the ZANIM and ZANIM-LN distributions. We develop data augmentation techniques for efficient sampling in Section 2.4, discuss prior specifications in Section 2.5, and provide a novel MCMC algorithm to perform posterior inference in Section 2.6.

2.1 The ZANIM and ZANIM-LN distributions

The main challenge in dealing with an excess of zeros in multivariate count-compositional settings, compared to univariate cases, is that the zero-inflation can occur in a single category or across multiple categories. Extreme cases where zeros co-occur in all but one category are said to exhibit N -inflation. In our recent research (Menezes et al., 2025), we provided new probabilistic characterisations of zero-inflated extensions of the multinomial and DM distributions, deriving their probability mass function (PMF) and other key statistical properties. The proposed framework represents both distributions as finite mixture distributions with 2^d components, which share a total of $2d$ parameters.

In particular, the zero-and- N -inflated multinomial (ZANIM) distribution introduced by Menezes et al. (2025), is characterised by the following stochastic representation:

$$(z_{ij} \mid \zeta_j) \stackrel{\text{ind.}}{\sim} \text{Bernoulli}[1 - \zeta_j], \quad j \in \{1, \dots, d\}, \quad (1)$$

$$(\mathbf{Y}_i \mid N_i, \boldsymbol{\theta}, \mathbf{z}_i) \sim \begin{cases} \delta_{\mathbf{0}_d}(\cdot), & \text{if } z_{ij} = 0 \forall j, \\ \text{Multinomial}_d [N_i, \vartheta_{i1}, \dots, \vartheta_{id}], & \text{otherwise,} \end{cases}$$

where $\delta_{\mathbf{0}_d}(\cdot)$ denotes the Dirac measure with unit mass at $\mathbf{0}_d$ and

$$\vartheta_{ij} = \frac{z_{ij}\theta_j}{\sum_{k=1}^d z_{ik}\theta_k}, \quad j \in \{1, \dots, d\},$$

such that the individual-level count probabilities $\boldsymbol{\vartheta}_i = (\vartheta_{i1}, \dots, \vartheta_{id})$ are functions of the category-specific parameters θ_j and ζ_j , which represent the population-level count and structural zero probabilities, respectively. Notably, $\boldsymbol{\vartheta}_i$ exhibits spikes at zero induced by the latent at-risk indicators \mathbf{z}_i , which in turn depend *a priori* on the ζ_j parameters. We stress that $\boldsymbol{\vartheta}_i$ describe within- and between-subject heterogeneity, while $\boldsymbol{\theta}$ characterises the counts at a global level.

The ZANIM distribution, due to its finite mixture nature, can handle overdispersion and — unlike the multinomial distribution — allow for positive covariance between the categories. We refer to Menezes et al. (2025) for further details on its PMF and its statistical properties. We note that Menezes et al. (2025) also provided a finite mixture representation and derived the PMF and statistical properties for the zero-and- N -inflated Dirichlet-multinomial (ZANIDM) distribution. This distribution was first introduced, in the form of a stochastic representation only, by Koslovsky (2023), who referred to it as the zero-inflated Dirichlet-multinomial (ZIDM).

Moving beyond [Menezes et al. \(2025\)](#), we propose the ZANIM-Lognormal (ZANIM-LN) distribution as an extension of ZANIM by incorporating log-linear multivariate Gaussian random effects on the compositional probabilities $\boldsymbol{\theta}$. Specifically, we introduce $\mathbf{u}_i \sim \text{Normal}_d[\mathbf{0}, \boldsymbol{\Sigma}_U]$ through the parameterisation $\theta_{ij} = \alpha_j e^{u_{ij}} / \sum_{k=1}^d \alpha_k e^{u_{ik}}$, where $\alpha_j > 0$ is a category-specific concentration parameter. Clearly, the ZANIM-LN distribution is richer than ZANIM since it allows for a general class of covariance through the specification of a hyperprior on $\boldsymbol{\Sigma}_U$. Consequently, α_j now serves as the population-level parameter while θ_{ij} inherits the subject-specific variability of the random effect u_{ij} . This enables the model to more flexibly capture category-specific overdispersion, which can help to account for sampling zeros, as an addition to the explicit mixture components in ZANIM for handling structural zeros. In Section 2.5, we present a factor-analytic hyperprior for the random effects that allows for parsimonious specification of the covariance matrix $\boldsymbol{\Sigma}_U$.

The ZANIM-LN distribution has some special cases of interest. When $\boldsymbol{\zeta} = \mathbf{0}_d$, we recover the multinomial distribution with log-normal random effects. When $\mathbf{u}_i = \mathbf{0}_d \forall i$, we obtain the aforementioned ZANIM distribution, and when both the random effects and zero-inflation parameters are all fixed at zero, we recover the usual multinomial distribution. In the Supplementary Material, we compare the marginal PMFs and theoretical moments of the ZANIM, ZANIM-LN, and ZANIDM distributions under parameter settings where all three distributions share the same expectations. We note that ZANIM-LN accommodates more overdispersed counts while capturing zero- and N -inflation under the finite mixture framework of [Menezes et al. \(2025\)](#).

2.2 Overview of the nonparametric BART priors

We now present a brief review and establish the notation for the nonparametric BART prior introduced by [Chipman et al. \(2010\)](#) and the log-linear BART extension proposed by [Murray \(2021\)](#). These nonparametric priors underpin the novel Bayesian models for count-compositional developed in the subsequent sections. In BART, an unknown function $f(\mathbf{x}_i)$ of interest is represented as a sum of m decision trees $f(\mathbf{x}_i) = \sum_{h=1}^m g(\mathbf{x}_i, \mathcal{T}_h, \mathcal{M}_h)$, where each decision tree function $g(\mathbf{x}_i, \mathcal{T}_h, \mathcal{M}_h)$ is parametrised by a binary tree structure \mathcal{T}_h consisting of the tree topology with terminal and internal nodes denoted by \mathcal{L}_h and \mathcal{B}_h , respectively, and terminal node parameters \mathcal{M}_h . For each internal node $b \in \mathcal{B}_h$, there is a splitting rule of the form $[x_{jb} \leq c_b]$. The terminal node parameters are defined as $\mathcal{M}_h = \{\mu_{ht} : t \in \mathcal{L}_h\}$, where $\mu_{ht} \in \mathbb{R}$. The tree structure \mathcal{T}_h , represented by a sequence of decision rules, induces a partition $\{\mathcal{A}_{h1}, \dots, \mathcal{A}_{hb_h}\}$ of the covariate space \mathcal{X} . Each element of the partition corresponds to a terminal node of the tree. Given $(\mathcal{T}_h, \mathcal{M}_h)$, the regression tree function can thus be expressed as a step function given by $g(\mathbf{x}_i, \mathcal{T}_h, \mathcal{M}_h) = \mathbb{1}(\mathbf{x}_i \in \mathcal{A}_{ht})\mu_{ht}$, for $t \in \mathcal{L}_h$.

The number of trees m in the ensemble is considered as a specified hyperparameter with typical large values of 50, 100, or 200 often giving reasonable performance (see, e.g., [Bleich et al., 2014](#); [Chipman et al., 2010](#); [Sparapani et al., 2023](#)). The BART prior on $f(\mathbf{x}_i)$ is formulated to impose regularisation and prevent overfitting. It is assumed that the trees are independent and the terminal nodes are conditionally independent given the trees, i.e., $\pi(\mathcal{T}, \mathcal{M}) = \prod_{h=1}^m \pi_{\mathcal{T}}(\mathcal{T}_h) \pi_{\mathcal{M}}(\mathcal{M}_h \mid \mathcal{T}_h)$. For $\pi_{\mathcal{T}}(\mathcal{T}_h)$, the most common choice to control the tree depth, which we adopt here, is the branching process prior proposed by [Chipman et al. \(1998\)](#). For the splitting rules $[x_{jb} < c_b]$ associated to each internal node $b \in \mathcal{B}_h$, the following procedure is suggested: (i) sample a covariate index j_b uniformly from $\{1, \dots, p\}$ and then (ii) sample a split value c_b uniformly from those that yield a valid partition. If no such valid splitting rule exists, the node is forced to be terminal. For the terminal node parameters \mathcal{M}_h , it is assumed that $\pi_{\mathcal{M}}(\mathcal{M}_h \mid \mathcal{T}_h) = \prod_{t \in \mathcal{L}_h} \pi_{\mu}(\mu_{ht})$, where π_{μ} is chosen so that it is conditionally conjugate.

[Chipman et al. \(2010\)](#) proposed an inference procedure for the BART parameters $\{(\mathcal{T}_h, \mathcal{M}_h)\}_{h=1}^m$ using MCMC methods with a tailored version of Bayesian backfitting ([Hastie and Tibshirani, 2000](#)). Conditional on $\{(\mathcal{T}_\ell, \mathcal{M}_\ell)\}_{\ell \neq h}$, a block update on $(\mathcal{T}_h, \mathcal{M}_h)$ is performed, which consists of two steps: (i) update the tree topology \mathcal{T}_h from the conditional distribution of $(\mathcal{T}_h \mid \mathcal{T}_{(h)}, \mathcal{M}_{(h)}, \dots)$ using a Metropolis-Hastings (MH) step with transition kernels proposed by [Chipman et al. \(1998\)](#), (ii) sample the terminal node parameters \mathcal{M}_h from their full conditional distribution $\pi(\mathcal{M}_h \mid \mathcal{T}_h, \mathcal{T}_{(h)}, \mathcal{M}_{(h)}, \dots)$. See [Chipman et al. \(2010\)](#) for further details of the sampling strategy and an extension which incorporates a probit link function for binary responses.

The log-linear BART prior of [Murray \(2021\)](#) reparameterises the terminal node parameters via $\lambda_{ht} = e^{\mu_{ht}}$, where $\lambda_{ht} > 0$, such that $\Lambda_h = \{\lambda_{ht}: t \in \mathcal{L}_h\}$. Thus, the prior can be expressed as $\log [f(\mathbf{x}_i)] = \sum_{h=1}^m \log [g(\mathbf{x}_i; \mathcal{T}_h, \Lambda_h)] = \sum_{h=1}^m \log(\lambda_{ht}) \mathbb{1}(\mathbf{x}_i \in \mathcal{A}_{ht})$, where $t \in \mathcal{L}_h$. According to [Murray \(2021\)](#), this prior can be used for any probability distribution which has a (possibly augmented) likelihood of the form

$$\mathcal{L}(\mathcal{T}, \Lambda; \mathbf{y}, \mathbf{x}, \dots) = \prod_{i=1}^n v_i f(\mathbf{x}_i)^{\kappa_i} \exp [\nu_i f(\mathbf{x}_i)], \quad (2)$$

where v_i , κ_i , and ν_i are functions of data \mathbf{y} or latent variables. In particular, [Murray \(2021\)](#) shows that, after appropriate data augmentation, the multinomial distribution admits an augmented likelihood that factorises across the categories and takes the form in (2) for each category. [Murray \(2021\)](#) refers to this model as multinomial logistic BART and evaluates its performance in multi-classification settings, where $N_i = 1$. Under the wider log-linear BART framework, the prior for the parameters $\{(\mathcal{T}_h, \Lambda_h)\}_{h=1}^m$ has the same independence assumption across the trees as [Chipman et al. \(2010\)](#) and thus factorises via $\pi(\mathcal{T}_h, \Lambda_h) = \pi_{\mathcal{T}}(\mathcal{T}_h) \pi_{\Lambda}(\Lambda_h | \mathcal{T}_h)$, where $\pi_{\Lambda}(\Lambda_h | \mathcal{T}_h) = \prod_{t \in \mathcal{L}_h} \pi_{\lambda}(\lambda_{ht})$ and π_{Λ} is chosen to maintain conditional conjugacy, in the spirit of the standard BART.

2.3 The ZANIM-BART and ZANIM-LN-BART models

Building on the BART frameworks above, and the zero-inflated count-compositional distributions described in Section 2.1, we adopt the log-linear BART prior of [Murray \(2021\)](#) and the probit-BART prior of [Chipman et al. \(2010\)](#) to propose two novel nonparametric models: ZANIM-BART and ZANIM-LN-BART. Specifically, under the ZANIM-LN distribution, we assume the log-linear BART prior of [Murray \(2021\)](#) for θ_i , such that the subject-specific count probability of category j becomes covariate-dependent via

$$\theta_{ij} = \frac{f_j^{(c)}(\mathbf{x}_i) e^{u_{ij}}}{\sum_{k=1}^d f_k^{(c)}(\mathbf{x}_i) e^{u_{ik}}}, \quad \log f_j^{(c)}(\mathbf{x}_i) = \sum_{h=1}^{m_{\theta}} \log \left[g \left(\mathbf{x}_i; \mathcal{T}_{hj}^{(c)}, \Lambda_{hj} \right) \right], \quad (3)$$

where $\mathcal{T}_{hj}^{(c)}$ denotes the h -th binary tree topology for the category j and $\Lambda_{hj} = \{\lambda_{htj}: \mathcal{L}_{hj}^{(c)}\}$ denotes the corresponding set of terminal node parameters.

We further consider the probit-BART prior of [Chipman et al. \(2010\)](#) for ζ , such that the covariate-dependent structural zero probability for category j is given by

$$\zeta_{ij} = \Phi \left(f_j^{(0)}(\mathbf{x}_i) \right) = \Phi \left[\sum_{h=1}^{m_{\zeta}} g \left(\mathbf{x}_i; \mathcal{T}_{hj}^{(0)}, \mathcal{M}_{hj} \right) \right], \quad (4)$$

where $\Phi(\cdot)$ is the standard normal cumulative distribution function, and $\mathcal{T}_{hj}^{(0)}$ and $\mathcal{M}_{hj} = \{\mu_{htj}: \mathcal{L}_{hj}^{(0)}\}$ are the category-specific tree structure and terminal node parameters, respectively. Setting $u_{ij} = 0$ in (3) recovers the ZANIM-BART model, which also adopts (4) for the structural zero probabilities. It is worth noting that our models assign independent BART priors $f_j^{(c)}$ and $f_j^{(0)}$, for all categories $j \in \{1, \dots, d\}$, to both the compositional and structural zero probability parameters of the ZANIM and ZANIM-LN distributions. Consequently, the ZANIM-BART model generalises the multinomial logistic BART model of [Murray \(2021\)](#) by introducing independent BART priors $f_j^{(0)}$ for the structural zero probabilities and ZANIM-LN-BART further extends this framework by incorporating subject-specific log-linear multivariate Gaussian random effects.

2.4 Likelihood formulations

We now derive the augmented likelihood function for the ZANIM-LN-BART model. This derivation plays a fundamental role in our methodological contribution, as it enables the development of an efficient MCMC algorithm for sampling the model parameters. The corresponding augmented likelihood function for the ZANIM-BART model can be obtained by setting the random effect terms u_{ij} to 0 in the expressions which follow.

Let $\mathbf{f}^{(c)} = (f_1^{(c)}, \dots, f_d^{(c)})$ and $\mathbf{f}^{(0)} = (f_1^{(0)}, \dots, f_d^{(0)})$ denote the independent BART priors which characterise the ZANIM-LN-BART model defined in (3) and (4). We build on (1) using two steps of data augmentation. First, we adapt the data augmentation scheme proposed by [Menezes et al. \(2025, see Supplementary Material S.1 for details\)](#) for the ZANIM distribution, by introducing the sample-specific latent variables

$$\left(\phi_i \mid \mathbf{y}_i, \mathbf{z}_i, \mathbf{u}_i, \mathbf{f}^{(c)} \right) \stackrel{\text{ind.}}{\sim} \text{Gamma} \left[N_i, \sum_{j=1}^d z_{ij} f_j^{(c)}(\mathbf{x}_i) e^{u_{ij}} \right]. \quad (5)$$

This construction yields the following augmented likelihood for $\mathbf{f}^{(c)}$ and $\mathbf{f}^{(0)}$, which notably factorises over the categories $j \in \{1, \dots, d\}$:

$$\begin{aligned} \mathcal{L} \left(\mathbf{f}^{(c)}, \mathbf{f}^{(0)}; \mathbf{y}, \mathbf{x}, \mathbf{u}, \mathbf{z}, \boldsymbol{\phi} \right) &\propto \prod_{i=1}^n \prod_{j=1}^d \left\{ \left[\Phi \left(f_j^{(0)}(\mathbf{x}_i) \right) \right]^{1-z_{ij}} \left[1 - \Phi \left(f_j^{(0)}(\mathbf{x}_i) \right) \right]^{z_{ij}} \right. \\ &\quad \times \left. \left[f_j^{(c)}(\mathbf{x}_i) \right]^{y_{ij}} e^{-\phi_i z_{ij} e^{u_{ij}} f_j^{(c)}(\mathbf{x}_i)} \right\}. \end{aligned} \quad (6)$$

Importantly, the BART priors $f_j^{(c)}$ and $f_j^{(0)}$ are conditionally independent given the data and the latent variables and the terms involving $f_j^{(c)}$ admit a form analogous to the generic likelihood function of the log-linear BART prior in (2).

In the second step, to simplify the terms of the zero-inflation component in (6), we follow the probit BART model of [Chipman et al. \(2010\)](#) and apply the data augmentation scheme of [Albert and Chib \(1993\)](#). However, we stress that the binary response itself, z_{ij} , is also latent in our case. Specifically, we introduce further latent variables w_{ij} , where $w_{ij} \sim \text{TN}_{[-\infty, 0]}[f_j^{(0)}(\mathbf{x}_i), 1]$ when $z_{ij} = 1$ and $w_{ij} \sim \text{TN}_{[0, \infty)}[f_j^{(0)}(\mathbf{x}_i), 1]$ when $z_{ij} = 0$ (which corresponds to a structural zero), where $\text{TN}_{[a, b]}[\mu, \sigma^2]$ denotes the truncated normal distribution on the interval $[a, b]$ with location μ and scale parameter σ . The resulting augmented likelihood takes the form

$$\mathcal{L} \left(\mathbf{f}^{(c)}, \mathbf{f}^{(0)}; \mathbf{y}, \mathbf{x}, \mathbf{u}, \mathbf{z}, \mathbf{w}, \boldsymbol{\phi} \right) \propto \prod_{i=1}^n \prod_{j=1}^d \left\{ \varphi \left(w_{ij}; f_j^{(0)}(\mathbf{x}_i), 1 \right) \left[f_j^{(c)}(\mathbf{x}_i) \right]^{y_{ij}} e^{-\phi_i z_{ij} e^{u_{ij}} f_j^{(c)}(\mathbf{x}_i)} \right\}, \quad (7)$$

where $\varphi(x; \mu, \sigma^2)$ is the Gaussian probability density function with mean μ and variance σ^2 . Finally, we note that the full conditional distribution of the latent variables z_{ij} , given y_{ij} , u_{ij} , ϕ_i , $f_j^{(c)}$, and $f_j^{(0)}$, follows

$$(z_{ij} \mid \dots) \stackrel{\text{ind.}}{\sim} \begin{cases} \text{Bernoulli} \left[\frac{\left[1 - \Phi \left(f_j^{(0)}(\mathbf{x}_i) \right) \right] e^{-\phi_i u_{ij} f_j^{(c)}(\mathbf{x}_i)}}{\Phi \left(f_j^{(0)}(\mathbf{x}_i) \right) + \left[1 - \Phi \left(f_j^{(0)}(\mathbf{x}_i) \right) \right] e^{-\phi_i u_{ij} f_j^{(c)}(\mathbf{x}_i)}} \right], & \text{if } y_{ij} = 0, \\ 1, & \text{otherwise.} \end{cases} \quad (8)$$

These factorisations play a central role in our MCMC schemes, discussed later in Section 2.6, as they allow us to sample the parameters $\{\mathcal{T}_{jh}^{(c)}, \Lambda_{jh}\}$ and $\{\mathcal{T}_{jh}^{(0)}, \mathcal{M}_{jh}\}$ using established BART sampling routines. We refer the reader to the Supplementary Material for more details.

2.5 Prior specifications

A key aspect of the BART framework is the adoption of regularisation priors which shrink the contribution of each terminal node to the final prediction produced by the overall additive ensemble. This prevents any one tree from dominating and helps to mitigate against overfitting. This principle also applies to the extensions of BART which we use as nonparametric priors in our ZANIM-BART and ZANIM-LN-BART models.

We recall that both models incorporate category-specific regression trees for both the compositional and structural zero probabilities, with the corresponding parameters $\{\mathcal{T}_{jh}^{(c)}, \Lambda_{jh}\}_{h=1}^{m_\theta}$ and $\{\mathcal{T}_{jh}^{(0)}, \mathcal{M}_{jh}\}_{h=1}^{m_\zeta}$. For the priors on the tree topologies $\mathcal{T}_{jh}^{(c)}$ and $\mathcal{T}_{jh}^{(0)}$, we adopt the branching process prior introduced by [Chipman et al. \(1998\)](#), with the hyperparameter values recommended by [Chipman et al. \(2010\)](#). To sample a covariate

index for forming the splitting rules of the trees, in our default implementation we sample uniformly from the p available predictors with probability $\mathbf{s} = (s_1, \dots, s_p)$, where $s_k = 1/p \forall k \in \{1, \dots, p\}$. In the microbiome case study in Section 4.1, we instead adopt the sparsity-inducing prior of [Linero \(2018\)](#) which assumes $\mathbf{s} \sim \text{Dirichlet}[\omega/p, \dots, \omega/p]$, with an additional hyperprior on $\omega/(\omega + \rho) \sim \text{Beta}[a_\omega, b_\omega]$, where we follow [Linero \(2018\)](#) and set $a_\omega = 0.5$, $b_\omega = 1$, and $\rho = p$.

Given the tree topologies $\mathcal{T}_{hj}^{(c)}$ and $\mathcal{T}_{hj}^{(0)}$, we follow [Murray \(2021\)](#) and [Chipman et al. \(2010\)](#) by assuming conditionally conjugate priors for $\{\Lambda_{hj}\}_{h=1}^{m_\theta}$ and $\{\mathcal{M}_{hj}\}_{h=1}^{m_\zeta}$. For the terminal node parameters $\{\Lambda_{hj}\}_{h=1}^{m_\theta}$ of the BART priors associated with the compositional probabilities, we consider $\lambda_{htj} \stackrel{\text{ind.}}{\sim} \text{Gamma}[c_0, d_0]$ and calibrate this in accordance with the recommendations of [Murray \(2021\)](#) for the multinomial logistic BART model. Specifically, we consider that each $f_j^{(c)}$ has the same number of trees m_θ and, through the normal approximation of the log-odds between two distinct categories, obtain the hyperparameters c_0 and d_0 in such a way that $\mathbb{E}[\lambda_{htj}] = 0$ and $\text{Var}[\lambda_{htj}] = a_\lambda^2/m_\theta$, where a_λ is a tuning parameter. Solving for c_0 and d_0 , we obtain expressions in terms of the digamma and trigamma functions: $d_0 = \exp\{(\ln \Gamma)'(c_0)\}$ and $(\ln \Gamma)''(c_0) = a_\lambda^2/m_\theta$, where the last equation is computed using the Newton-Raphson algorithm. Although the choice of $a_\lambda = 3.5/\sqrt{2}$ suggested by [Murray \(2021\)](#) works reasonably well in practice, we follow [Linero et al. \(2020\)](#) by assuming the hyperprior $a_\lambda \sim \text{half-Cauchy}[0, 1]$ and updating a_λ using slice sampling, in order to allow the model to determine the amount of variability according to the data. Regarding the terminal node parameters $\{\mathcal{M}_{hj}\}_{h=1}^{m_\zeta}$ in the BART priors describing the structural zero probabilities, the conjugate priors are $\mu_{htj} \stackrel{\text{ind.}}{\sim} \text{Normal}[0, \sigma_\mu^2]$. We proceed as per [Chipman et al. \(2010\)](#) by shrinking each category-specific $f_j^{(0)}$ towards zero by setting $\sigma_\mu = 0.5/(k\sqrt{m_\zeta})$, where $k = 2$ is such that $f_j^{(0)}$ has high prior probability of lying in $(-3.0, 3.0)$. For the numbers of trees m_θ and m_ζ of each $f_j^{(c)}$ and $f_j^{(0)}$, respectively, we use $m_\theta = m_\zeta = 200$, following the recommendation of [Chipman et al. \(2010\)](#).

The ZANIM-LN-BART model has multivariate Gaussian random effects, \mathbf{u}_i , with d -dimensional covariance matrix $\boldsymbol{\Sigma}_U$. However, $\boldsymbol{\Sigma}_U$ is singular because the parameters θ_{ij} in (3) lie on the d -dimensional continuous simplex space \mathbb{S}_d . To address this identifiability issue, we use a sum-to-zero constraint and transform \mathbf{u}_i into the $(d-1)$ -dimensional vector \mathbf{v}_i by setting $\mathbf{u}_i = \mathbf{B}\mathbf{v}_i$, where \mathbf{B} is $d \times (d-1)$ orthogonal matrix, such that $\text{Var}[\mathbf{u}_i] = \boldsymbol{\Sigma}_U = \mathbf{B}\boldsymbol{\Sigma}_V\mathbf{B}^\top$. We conclude the specification of ZANIM-LN-BART model by placing a factor-analytic hyperprior on the latent variables \mathbf{v}_i via the decomposition $\mathbf{v}_i = \boldsymbol{\Gamma}\boldsymbol{\eta}_i + \boldsymbol{\epsilon}_i$, where $\boldsymbol{\Gamma} = [\gamma_{jk}]_{j=1, \dots, d-1}^{k=1, \dots, q}$ is a $(d-1) \times q$ factor loadings matrix, $\boldsymbol{\eta}_i \sim \text{Normal}_q[\mathbf{0}_q, \mathbf{I}_q]$, and $\boldsymbol{\epsilon}_i \sim \text{Normal}_{d-1}[\mathbf{0}_{d-1}, \boldsymbol{\Psi}]$, with $\boldsymbol{\Psi} = \text{diag}(\psi_1, \dots, \psi_{d-1})$. Regarding the specification of q , we fix an upper limit for the number of loadings columns as the Ledermann bound ([Anderson and Rubin, 1956](#)) and shrink the contributions of the redundant loadings columns by employing the nonparametric multiplicative gamma process shrinkage prior of [Bhattacharya and Dunson \(2011\)](#). By doing so, we obviate the need to pre-specify a fixed number of latent factors. This prior has been adopted in a wide range of settings, including model-based clustering ([Murphy et al., 2020](#)), Bayesian partial least squares regression ([Urbas et al., 2024](#)), and the modelling of count-compositional data ([Ren et al., 2017](#)). See the Supplementary Material for further details of the corresponding full conditional distributions.

Notably, dimension-reduction of latent multivariate Gaussian random effects has also been considered in other modelling frameworks designed for count-compositional data. [Zeng et al. \(2023\)](#), for example, employs probabilistic principal component analysis, which can be recovered under our approach by setting $\boldsymbol{\Psi} = \psi \mathbf{I}_{d-1}$. Our allowance for uncommon idiosyncratic variances is designed to better capture category-specific levels of excess variability. Our approach also differs via the imposition of a sum-to-zero constraint, which treats all categories equally, whereas [Zeng et al. \(2023\)](#) address the non-identifiability of the covariance matrix via an inherently asymmetric additive log-ratio transformation, which requires a reference category.

2.6 Posterior inference

With the likelihood and priors formulated, we now derive our MCMC algorithm by leveraging the Bayesian backfitting algorithm of [Chipman et al. \(2010\)](#) and the generalised Bayesian backfitting algorithm of [Murray \(2021\)](#) to sample $\{\mathcal{T}_{hj}^{(c)}, \Lambda_{hj}\}_{h=1}^{m_\theta}$ and $\{\mathcal{T}_{hj}^{(0)}, \mathcal{M}_{hj}\}_{h=1}^{m_\zeta}$, respectively. This is facilitated by the factorisation of

the augmented likelihood in (7), which allows conditionally independent updates to be carried out across the categories $j \in \{1, \dots, d\}$, for each $f_j^{(c)}$ and $f_j^{(0)}$. Again, we derive the algorithm for the ZANIM-LN-BART model and recall that ZANIM-BART is recovered as a special case by setting the random effects $u_{ij} = 0$. To implement these Bayesian backfitting schemes, we require the integrated likelihood functions for the trees and the full conditional distributions of the corresponding terminal node parameters.

We begin by deriving these quantities for the tree ensembles $f_j^{(c)}$ associated with the compositional probabilities. Let $\mathcal{T}_{(h)j}^{(c)}$ and $\Lambda_{(h)j}$ denote the tree topologies and the terminal node parameters for all trees of category j , excluding the h -th. Following Murray (2021), we denote by $f_{(h)j}^{(c)}(\mathbf{x}_i) = \prod_{\ell \neq h} g(\mathbf{x}_i; \mathcal{T}_{\ell j}^{(c)}, \Lambda_{\ell j}^{(c)})$ the fit from all but the h -th tree of category j . By integrating out Λ_{hj} from the augmented likelihood in (6) using their conditionally conjugate priors, it can be shown that

$$\pi(\mathcal{T}_{hj}^{(c)} | \mathcal{T}_{(h)j}^{(c)}, \Lambda_{(h)j}, \mathbf{y}, \mathbf{z}, \mathbf{u}, \boldsymbol{\phi}) \propto \pi_{\mathcal{T}}(\mathcal{T}_{hj}^{(c)}) \prod_{t \in \mathcal{L}_{hj}^{(c)}} \frac{d_0^{c_0}}{\Gamma(c_0)} \frac{\Gamma(r_{htj}^{(c)} + c_0)}{(s_{htj}^{(c)} + d_0)^{r_{htj}^{(c)} + c_0}}, \quad (9)$$

where $r_{htj}^{(c)} = \sum_{i: \mathbf{x}_i \in \mathcal{A}_{htj}^{(c)}} y_{ij}$ and $s_{htj}^{(c)} = \sum_{i: \mathbf{x}_i \in \mathcal{A}_{htj}^{(c)}} \phi_i z_{ij} e^{u_{ij}} f_{(h)j}^{(c)}(\mathbf{x}_i)$. Likewise, it follows that the full conditional distributions of the terminal node parameters Λ_{hj} , are

$$(\lambda_{thj} | \mathcal{T}_{hj}^{(c)}, \mathcal{T}_{(h)j}^{(c)}, \Lambda_{(h)j}, \mathbf{y}, \mathbf{z}, \mathbf{u}, \boldsymbol{\phi}) \stackrel{\text{ind.}}{\sim} \text{Gamma}\left[r_{htj}^{(c)} + c_0, s_{htj}^{(c)} + d_0\right], \quad t \in \mathcal{L}_{hj}^{(c)}. \quad (10)$$

Similarly, for the tree ensembles $f_j^{(0)}$ associated with the structural zero probabilities, we let $\mathcal{T}_{(h)j}^{(0)}$ and $\mathcal{M}_{(h)j}$ denote the tree topologies and corresponding terminal node parameters for all trees, except for the h -th, for category j . Following Chipman et al. (2010), let $r_{(h)ij} \equiv w_{ij} - \sum_{\ell \neq h} g(\mathbf{x}_i; \mathcal{T}_{\ell}^{(0)}, \mathcal{M}_{\ell})$ be the partial residuals, such that $(\mathcal{T}_{(h)j}^{(0)}, \mathcal{M}_{(h)j})$ only depends on the data through $\mathbf{r}_{(h)j} = (r_{(h)1j}, \dots, r_{(h)nj})$, where $r_{(h)ij} \sim \text{Normal}[g(\mathbf{x}_i; \mathcal{T}_{hj}^{(0)}, \mathcal{M}_{hj}), 1]$. After integrating out \mathcal{M}_{hj} from the augmented likelihood in (6), using their conditionally conjugate priors, we obtain

$$\pi(\mathcal{T}_{hj}^{(0)} | \mathbf{r}_{(h)j}) \propto \pi_{\mathcal{T}}(\mathcal{T}_{hj}^{(0)}) \prod_{t \in \mathcal{L}_{hj}^{(0)}} \left(\frac{1}{n_{htj} \sigma_{\mu}^2 + 1} \right)^{1/2} \exp \left[\frac{1}{2} \left(\frac{\sigma_{\mu}^2 (s_{htj}^{(0)})^2}{2(n_{htj} \sigma_{\mu}^2 + 1)} \right) \right], \quad (11)$$

where $s_{htj}^{(0)} = \sum_{i: \mathbf{x}_i \in \mathcal{A}_{htj}^{(0)}} r_{(h)ij}$ and n_{htj} is the total number of observations in the partition $\mathcal{A}_{htj}^{(0)}$. It can similarly be shown that the full conditional distributions of the terminal node parameters are

$$(\mu_{htj} | \mathcal{T}_{hj}^{(0)}, \mathbf{r}_{(h)j}) \stackrel{\text{ind.}}{\sim} \text{Normal}\left[\frac{s_{htj}^{(0)}}{n_{htj} + \sigma_{\mu}^2}, 1/(n_{htj} + 1/\sigma_{\mu}^2)\right], \quad t \in \mathcal{L}_{hj}^{(0)}. \quad (12)$$

Sampling from the tree topologies, $\mathcal{T}_h^{(c)}$ and $\mathcal{T}_h^{(0)}$, is carried out via MH using the respective integrated likelihood functions in (9) and (11). The tree proposals are generated through transition kernels defined as mixtures of birth, death, and change moves (for more details, see Kapelner and Bleich, 2016). Finally, we emphasise that the updates from the full conditional distributions of the latent variables ϕ_i given in (5), the latent zero-inflation indicators z_{ij} given in (8), and the truncated normal latent variables w_{ij} , form part of our MCMC algorithm. Additional sampling steps are required for ZANIM-LN-BART, where we update the random effects using elliptical slice sampling (Murray et al., 2010) and update the parameters of the factor-analytic hyperprior via closed-form Gibbs steps. Further details, along with pseudocode describing the MCMC algorithm for ZANIM-LN-BART, are provided in the Supplementary Material.

3 Simulations

Our simulation experiments have two main goals. First, we demonstrate the ability of the ZANIM-BART model to recover nonlinear relationships between one covariate and the observed composition in the presence

of structural zeros. Second, we evaluate the performance of the ZANIM-BART and ZANIM-LN-BART models against alternative models in a realistic count-compositional scenario where the data are not generated from any of the competing models. Where applicable, we compare ZANIM-BART and ZANIM-LN-BART with the ZIDM regression model with spike-and-slab priors (ZIDM-reg) of [Koslovsky \(2023\)](#) and the multinomial logistic BART model (multinomial-BART) of [Murray \(2021\)](#). All hyperparameters of the ZANIM-BART and ZANIM-LN-BART models are specified as described in Section 2.5 and we adopt the same hyperparameter values, where applicable, for the multinomial-BART model.

For ZIDM-reg, we use the author’s implementation available via the R package ZIDM at <https://github.com/mkoslovsky/ZIDM>. However, in the first simulation, which incorporates only one covariate, we use our own implementation of the ZIDM model without the spike-and-slab priors, which we refer to as the ZANIDM-reg model in reference to its finite mixture representation ([Menezes et al., 2025](#)). For the ZANIM-BART, ZANIM-LN-BART, multinomial-BART, and ZANIDM-reg models, we provide an implementation via the R package `zanicc` available from the repository at <https://github.com/AndrMenezes/zanicc>. For efficient computation, the core parts of the MCMC algorithms to fit the models are written in C++ using object-oriented programming and the `Rcpp` package ([Eddelbuettel, 2013](#)) is used to expose our classes into the R environment. All computations in this section and the real data illustrations in Section 4 were performed on a laptop with a 2.7GHz Intel Core i7-12700H processor and 16 GB of RAM running on a Unix-based system.

3.1 Recovering nonlinear covariate effects with structural zeros

To obtain preliminary insights and illustrate key features of our methodology, we present a simulated example to demonstrate that the ZANIM-BART model can effectively recover the true compositional and structural zero probabilities, when both depend on covariates through nonlinear functional forms. We consider a scenario with $d = 4$ categories, $n = 400$ observations, and for maximum simplicity, only one covariate x_i , with values placed uniformly over $[-1, 1]$. The compositional counts, \mathbf{Y}_i , were generated via the stochastic representation of ZANIM in (1), subject to the total counts N_i being sampled from a discrete uniform distribution defined on the interval $[100, 500]$. The compositional probabilities, θ_{ij} , and the zero-inflation probabilities, ζ_{ij} , were related to the covariate x_i via $\theta_{ij} = f_j^{(c)}(x_i) / \sum_{k=1}^d f_k^{(c)}(x_i)$ and $\zeta_{ij} = \Phi(\sin(2\pi x_i) + x_i^2 - \beta_j^{(0)})$, where $\log f^{(j)}(x_i) = \sum_{\ell=1}^b s_{j\ell}(x_i)\beta_{j\ell}^{(c)}$, with $s_{j\ell}(\cdot)$ denoting cubic B-spline basis functions with three knots. The coefficients $\beta_{j\ell}^{(c)}$ are sampled from a standard normal distribution and the baseline zero-inflation values are $\beta_j^{(0)} = (0.5, 1.0, 1.5, 2.0)$. In this scenario, all observed zero counts are structural and the proportions of zeros across the four categories are 0.500, 0.318, 0.185, and 0.090.

We compare our ZANIM-BART model against the multinomial-BART of [Murray \(2021\)](#) and demonstrate that explicitly modelling the structural zero probabilities is crucial to obtain accurate estimates of the compositional probabilities. We also fit the ZANIDM-reg model, which ignores nonlinearities on the population-level parameters and hence provides poor estimates of the covariate effects. The MCMC algorithms for all three models were run with 12,000 iterations, discarding the first 6,000 as burn-in. The total runtime for the ZANIM-BART, multinomial-BART, and ZANIDM-reg models were 142.42, 87.05, and 13.83 seconds, respectively.

[Fig. 1](#) and [Fig. 2](#) compare the true compositional probabilities, θ_{ij} , and the true zero-inflation probabilities, ζ_{ij} , respectively, at given predictor values x_i , against the corresponding posterior estimates from the multinomial-BART, ZANIM-BART, and ZANIDM-reg models. It is clear that the multinomial-BART and ZANIDM-reg models both fail to capture the underlying true behaviour. The multinomial-BART model exhibits up and down peaks as an attempt to account for the structural zeros in the data, demonstrating that not accounting for zero-inflation has a crucial impact on the estimates of the count probabilities. Although the ZANIDM-reg model explicitly models the zero-inflation mechanism, it produces linear estimates for ζ_{ij} and overly smooth, approximately linear estimates for θ_{ij} , reflecting the limitations imposed by its parametric linear regression assumptions. In contrast, the ZANIM-BART model provides accurate estimates of the true behaviour of θ_{ij} and ζ_{ij} (see [Fig. 2](#)), demonstrating the flexibility of the BART priors in recovering complex, unknown, nonlinear regression functions in zero-inflated count-compositional data.

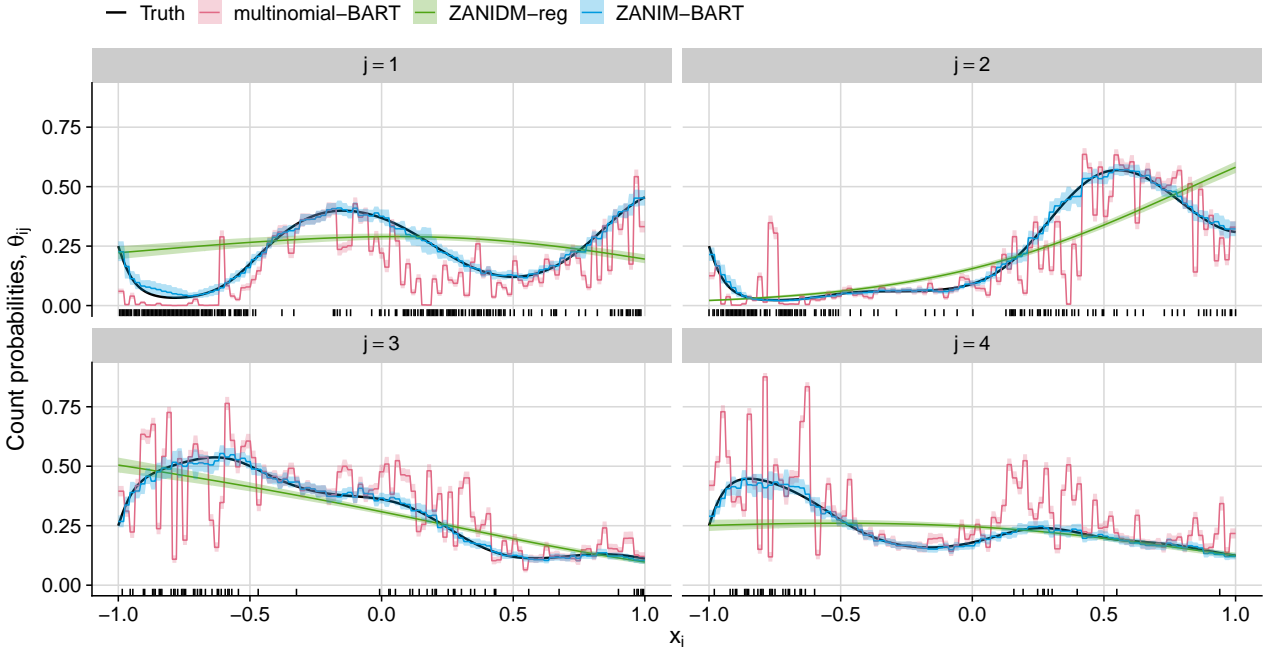


Fig. 1: Comparison of the multinomial-BART, ZANIDM-reg and ZANIM-BART models in estimating the true compositional probabilities θ_{ij} (black solid lines) for $d = 4$ categories. The posterior median and 95% credible intervals are given in each case. The rugs along the x -axes represent samples where the observed counts are zero.

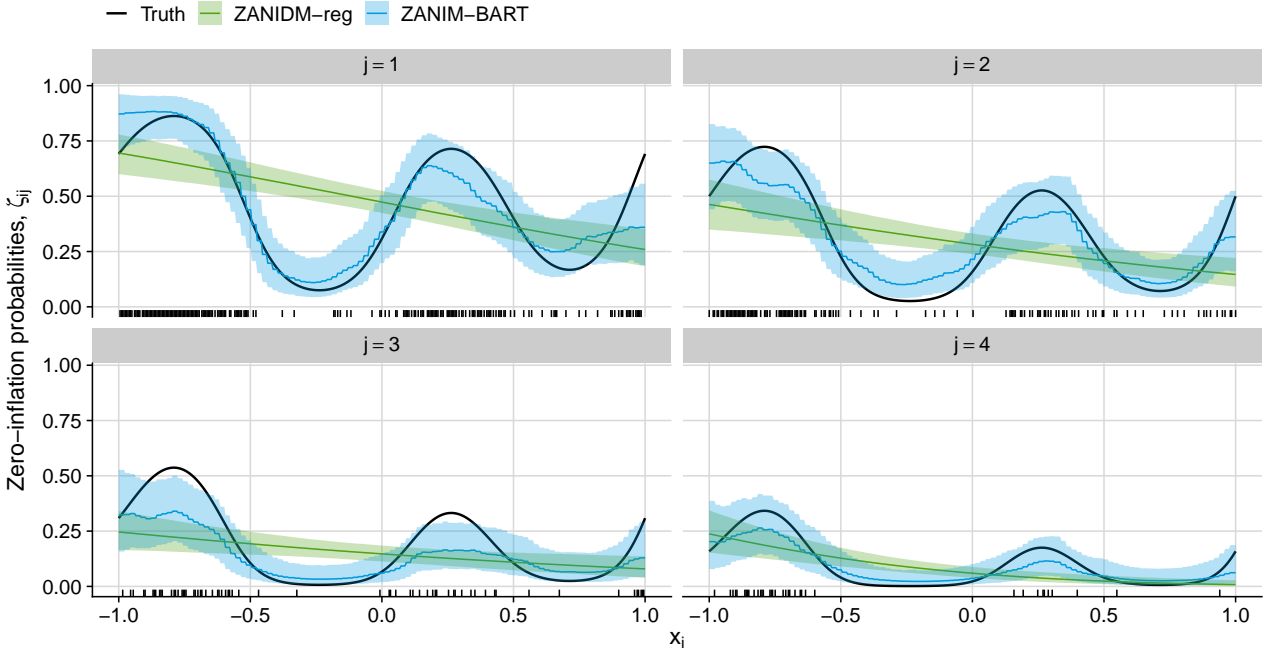


Fig. 2: ZANIDM-reg and ZANIM-BART estimates for the true zero-inflation probabilities ζ_{ij} (black solid lines) for $d = 4$ categories. The posterior median and 95% credible intervals are given in each case. The rugs along the x -axes represent samples where the observed counts are zero. Note that the multinomial-BART model is not included here as it does not include model components to capture zero-inflation.

3.2 Evaluation under model misspecification

We next evaluate the performance of the proposed ZANIM-BART and ZANIM-LN-BART models and the ZIDM-reg model of [Koslovsky \(2023\)](#), under a misspecified data generating process designed to reflect characteristics commonly observed in real count-compositional data sets. We consider $d = 20$ categories, different

sample sizes $n \in \{100, 500, 1000\}$, total counts N_i drawn uniformly from $[1000, 5000]$, and $p = 6$ covariates, $\mathbf{x}_i = (x_{i1}, \dots, x_{i6})$, generated from the standard normal distribution.

Following a similar simulation design of [Koslovsky \(2023\)](#), the compositional counts \mathbf{Y}_i are generated from Multinomial $[N_i, \boldsymbol{\vartheta}_i]$, where the individual-level count probabilities are given by $\vartheta_{ij} = z_{ij}\lambda_{ij}/\sum_{k=1}^d z_{ik}\lambda_{ik}$, with $z_{ij} \sim \text{Bernoulli}[1 - \zeta_{ij}]$ and $\lambda_{ij} \sim \text{Gamma}[(1 - \tau)\tau^{-1}\alpha_{ij}, 1]$, such that τ , which we set to $\tau = 0.01$, controls the degree of overdispersion. To accommodate different types of complexity in the relationships between the covariates \mathbf{x}_i and the parameters of the data generating process, we specify the true functional forms of ζ_{ij} and α_{ij} , for each category $j \in \{1, \dots, 20\}$, as follows:

$$\begin{aligned} \text{logit } \zeta_{ij} &= \beta_{0j}^{(\zeta)} + \beta_{1j}^{(\zeta)} x_{i1}^{(j)} + \sin(2\pi x_{i2}^{(j)}) + x_{i2}^{2(j)} + x_{i1}^{(j)} x_{i2}^{(j)}, \\ \log \alpha_{ij} &= \beta_{0j}^{(\alpha)} + \beta_{1j}^{(\alpha)} x_{i1}^{(j)} + \sin(2\pi x_{i2}^{(j)}) + x_{i2}^{2(j)} + x_{i1}^{(j)} x_{i2}^{(j)}, \end{aligned}$$

where superscripts with the j index are used to indicate that the covariates, which are randomly chosen from the $p = 6$ available covariates, are both category- and parameter-specific. To vary the degree of abundance across the categories, the intercepts for the compositional probabilities were drawn from $\beta_{0j}^{(\alpha)} \sim \text{Uniform}[-2.3, 2.3]$, while the baseline structural zero probabilities were sampled from $\beta_{0j}^{(\zeta)} \sim \text{Uniform}[-0.1, 1.5]$. The coefficients $\beta_{1j}^{(\zeta)}$ and $\beta_{1j}^{(\alpha)}$ were sampled from the interval $[-1.8, -1.2] \cup [1.2, 1.8]$, ensuring both positive and negative covariate effects. Thus, the same covariates can affect both the compositional and zero-inflation probabilities. The categories may share the same covariates and the functional forms for both parameters contain linear, nonlinear, and interaction effects. Under these settings, the simulated counts exhibit a considerable degree of zero-inflation, with approximately 36% of all observations being equal to zero, and varying degrees of overdispersion, with the empirical dispersion indices of the categories, $\text{DI}[Y_j] = \text{Var}[Y_j]/\mathbb{E}[Y_j]$, ranging from 277 to 1446. We stress that the counts are not simulated from any of the competing ZANIM-BART, ZANIM-LN-BART, or ZIDM-reg models. Moreover, the underlying distributional assumption is neither ZANIM nor ZANIM-LN and the covariate effects are not represented by additive regression trees.

When fitting the models, we use all $p = 6$ available covariates across the category-specific regression structures. We run our MCMC algorithms with 10,000 iterations and discard the first 5,000. For the ZIDM-reg model with spike-and-slab priors, we use the `ZIDM::ZIDMbvs.R` function and run the MCMC algorithm of [Koslovsky \(2023\)](#) with 60,000 iterations, thinning every 10. We then discard the first 1,000 samples and use the remaining 5,000 posterior samples for inference.

To assess the parameter recovery of the models, we compute the Kullback-Leibler (KL) divergences between the true values and the corresponding posterior distributions, for both the compositional probabilities, $\theta_{ij} = \alpha_{ij}/\sum_{k=1}^d \alpha_{ik}$, and the structural zero probabilities, ζ_{ij} . For a given MCMC iteration t , we denote these two quantities by $\text{KL}(\boldsymbol{\theta}^{(t)})$ and $\text{KL}(\boldsymbol{\zeta}^{(t)})$, respectively. For the latter, we further average over the category-specific KL divergences, i.e., $\text{KL}(\boldsymbol{\zeta}^{(t)}) = 1/d \sum_{j=1}^d \text{KL}(\zeta_j^{(t)})$. The calculation of these aggregate measures follows from the definition of KL divergence along with an additional step of Monte Carlo integration performed at the observational level. As a measure of goodness-of-fit, we also calculate the average ranked probability score (RPS; [Murphy, 1970](#)) based on the marginal empirical cumulative distribution function (ECDF) of the true relative abundances, y_{ij}/N_i , and the corresponding posterior predictive distributions under all three models.

[Fig. 3](#) shows traceplots of $\text{KL}(\boldsymbol{\theta}^{(t)})$ and $\text{KL}(\boldsymbol{\zeta}^{(t)})$ under all three models, for a sample size of $n = 500$, in Panels **A** and **B**, respectively. It is clear that ZANIM-BART and ZANIM-LN-BART give similar results and yield substantially lower values than the ZIDM-reg model. For both sets of parameters, ZIDM-reg also exhibits much poorer mixing. Similar conclusions can be drawn from the results with sample sizes of $n = 100$ and $n = 1000$; we defer the corresponding traceplots to the Supplementary Material.

[Table 1](#) reports the KL divergences averaged over the MCMC draws for both $\boldsymbol{\theta}$ and $\boldsymbol{\zeta}$, along with the average RPS scores, for all sample sizes $n \in \{100, 500, 1000\}$ under all three models. We note that our ZANIM-BART and ZANIM-LN-BART models yield comparable results for all metrics, with ZANIM-LN-BART showing marginally better results in terms of goodness-of-fit (lowest RPS) and the recovery of structural zero

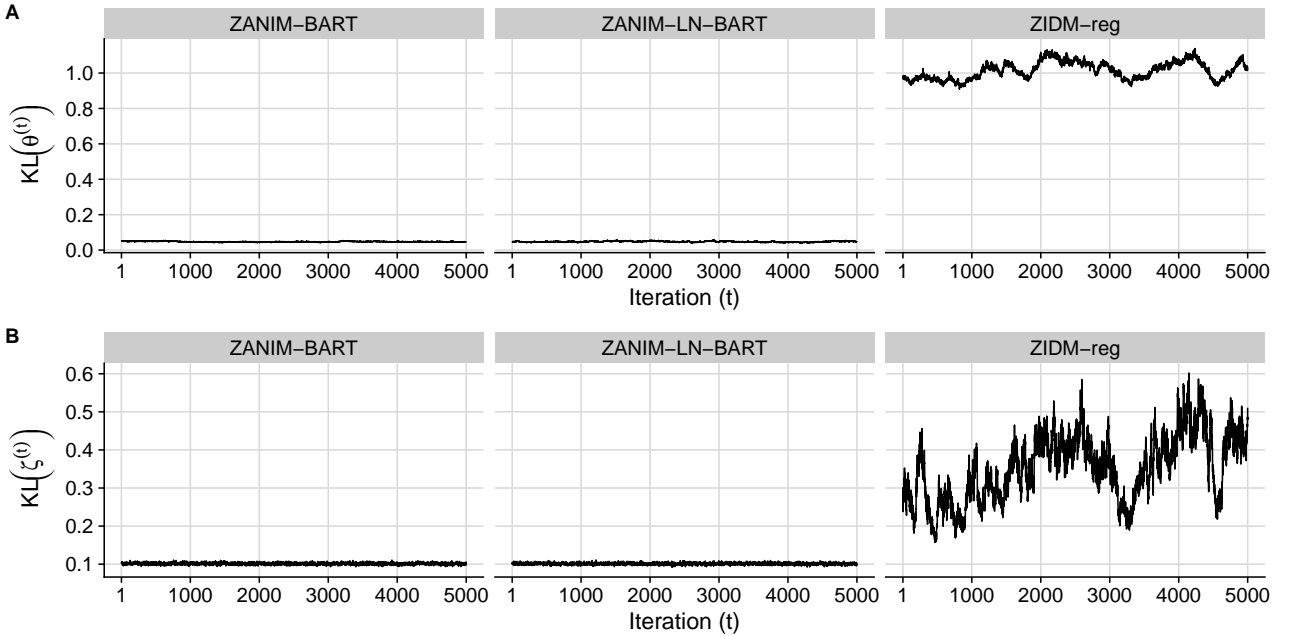


Fig. 3: Traceplots of $\text{KL}(\theta^{(t)})$ in Panel **A** and $\text{KL}(\zeta^{(t)})$ in Panel **B** under the ZANIM-BART, ZANIM-LN-BART, and ZIDM-reg models, for a sample size of $n = 500$.

probabilities, as implied by the lower $\text{KL}(\zeta)$ values, while ZANIM-BART performs slightly better at recovering the compositional probabilities, as indicated by the lower $\text{KL}(\theta)$ values. Moreover, both KL measures decrease as the sample size increases under our proposed models. In contrast, the ZIDM-reg model exhibits consistently worse performance, with the RPS and the KL divergences increasing as the sample size grows.

Table 1: Average rank probability scores and overall KL divergences, averaged over MCMC draws, categories, and observations, for the compositional (θ) and structural zero (ζ) probabilities under the ZANIM-BART, ZANIM-LN-BART, and ZIDM-reg models, for different sample sizes n . Lower is better for all metrics.

n	Model	RPS	$\text{KL}(\theta)$	$\text{KL}(\zeta)$
100	ZANIM-BART	0.0145	0.2805	0.1440
	ZANIM-LN-BART	0.0133	0.3088	0.1433
	ZIDM-reg	0.0350	0.9997	0.2989
500	ZANIM-BART	0.0163	0.0473	0.1013
	ZANIM-LN-BART	0.0158	0.0476	0.1012
	ZIDM-reg	0.0369	1.0151	0.3525
1000	ZANIM-BART	0.0161	0.0266	0.0763
	ZANIM-LN-BART	0.0159	0.0277	0.0758
	ZIDM-reg	0.0372	1.0223	0.5341

Overall, our simulation studies suggest that the established practical benefits of the standard BART model extend to our use of BART as a nonparametric prior in the ZANIM-BART and ZANIM-LN-BART models. In particular, the simulation results demonstrate that the BART prior is effective in recovering unknown smooth functions and low-order interactions. Moreover, despite the ability of ZIDM-reg model to accommodate structural zeros and overdispersion, it is fundamentally limited by its parametric linear regression assumptions. Indeed, its poor overall performance highlights the importance of simultaneously accounting for nonlinearities, interaction effects, and zero-inflation, as we do in our models.

4 Real data illustrations

The flexibility and usefulness of the ZANIM-BART and ZANIM-LN-BART models is demonstrated now through the analysis of two real count-compositional data sets with different characteristics. First, we show

that our models outperform the ZIDM-reg model of [Koslovsky \(2023\)](#) when analysing a benchmark human gut microbiome data set. Second, we illustrate the advantages of the ZANIM-LN-BART model in inferring climate effects from a large modern pollen-climate data set. In both case studies, all hyperparameters are set according to the guidelines given in Section 2.5.

4.1 Human gut microbiome data

The publicly available human gut microbiome data studied by [Wu et al. \(2011\)](#) has been used to motivate the development of new count-compositional models. For example, [Koslovsky \(2023\)](#) introduced the ZIDM regression model using these data. The data describe compositional counts of $d = 28$ genera-level operational taxonomic units from 16S rRNA sequencing of $n = 98$ individuals, along with $p = 97$ standardised dietary covariates obtained from a food frequency questionnaire. These data are characterised by substantial sparsity; 32.6% of the observed counts are zeros; by wide variation in the total counts, N_i , which range from 1183 to 15447; and by overdispersion, with the empirical dispersion index varying between 2.92 (*Actinomycineae*) and 4418.20 (*Prevotella*). Thus, this analysis not only provides a natural benchmark but also illustrates the novel features of the ZANIM-BART and ZANIM-LN-BART models; in particular, their ability to capture nonlinear covariate effects on both the population-level count and zero-inflation probabilities, which the ZIDM-reg model fails to accommodate. Our comparative analysis also includes the Dirichlet-multinomial regression (DM-reg) model with spike-and-slab prior of [Wadsworth \(2017\)](#).

In light of these data having a large number of covariates, we note that both the ZIDM-reg and DM-reg models have spike-and-slab priors on their regression coefficients in order to perform variable selection. For the ZIDM-reg model, this prior is assumed for both the count and zero-inflation levels of the model. Thus, in order to allow our ZANIM-BART and ZANIM-LN-BART models to perform variable selection for each category-specific set of population-level count and structural zero probabilities, we adopt the sparsity-inducing Dirichlet prior for decision tree splitting rules ([Linero, 2018](#)) described in Section 2.5. The MCMC algorithms of the ZANIM-BART and ZANIM-LN-BART models were run for 25,000 iterations, of which the first 20,000 were discarded as burn-in, resulting in 5,000 valid posterior samples for inference. For the ZIDM-reg and DM-reg models, we ran their MCMC algorithms for 100,000 iterations, discarding the first 5,000 and thinning every 10-th iteration. Additional analyses (which we defer to the Supplementary Material) indicate good mixing of the MCMC algorithms for all models.

We first assess goodness-of-fit based on the marginal ECDF of the observed relative abundances of each taxa, y_{ij}/N_i , and the corresponding posterior-predictive distributions obtained under the models. [Fig. 4](#) shows the results for the most abundant (*Bacteroides*) and most overdispersed (*Prevotella*) taxa. For *Bacteroides*, ZANIM-BART and ZANIM-LN-BART yield posterior-predictive distributions that are consistent with the observed data, in contrast to the ZIDM-reg and DM-reg models, which fail to adequately reproduce the observed abundances. For *Prevotella*, only the DM-reg model fails to capture the pattern in the observed data, providing evidence that explicitly modelling structural zeroes (as in the other three models) is crucial for these data. In the Supplementary Material, we report the RPS between the ECDF and corresponding posterior-predictive distributions for all taxa, showing that the ZANIM-LN-BART model outperforms the other models in the vast majority of cases.

We next perform a formal comparison of the ZANIM-BART, ZANIM-LN-BART, ZIDM-reg, and DM-reg models using the widely applicable information criterion (WAIC; [Watanabe, 2010](#)) defined here as $WAIC = -2(\sum_{i=1}^n \log \mathbb{E}[\Pr[\mathbf{Y}_i = \mathbf{y}_i | \mathbf{x}_i, \Theta]) - p_{waic}]$, where $p_{waic} = \sum_{i=1}^n \text{Var}[\log \Pr(\mathbf{Y}_i = \mathbf{y}_i | \mathbf{x}_i, \Theta)]$ is the estimated effective number of parameters, and the expectation and variance are with respect the posterior distribution over the model parameters denoted here by Θ , which include the trees and corresponding terminal node parameters for the ZANIM-BART and ZANIM-LN-BART models. Under mild regularity conditions, model selection based on the WAIC is asymptotically equivalent to leave-one-out cross-validation ([Watanabe, 2010](#)). We write $\Pr[\mathbf{Y}_i = \mathbf{y}_i | \cdot]$ for the model likelihood to emphasise that it is the PMF which is evaluated. A misconception about the ZIDM model is that it does not have a closed-form likelihood function ([Ascari et al., 2025](#)). However,

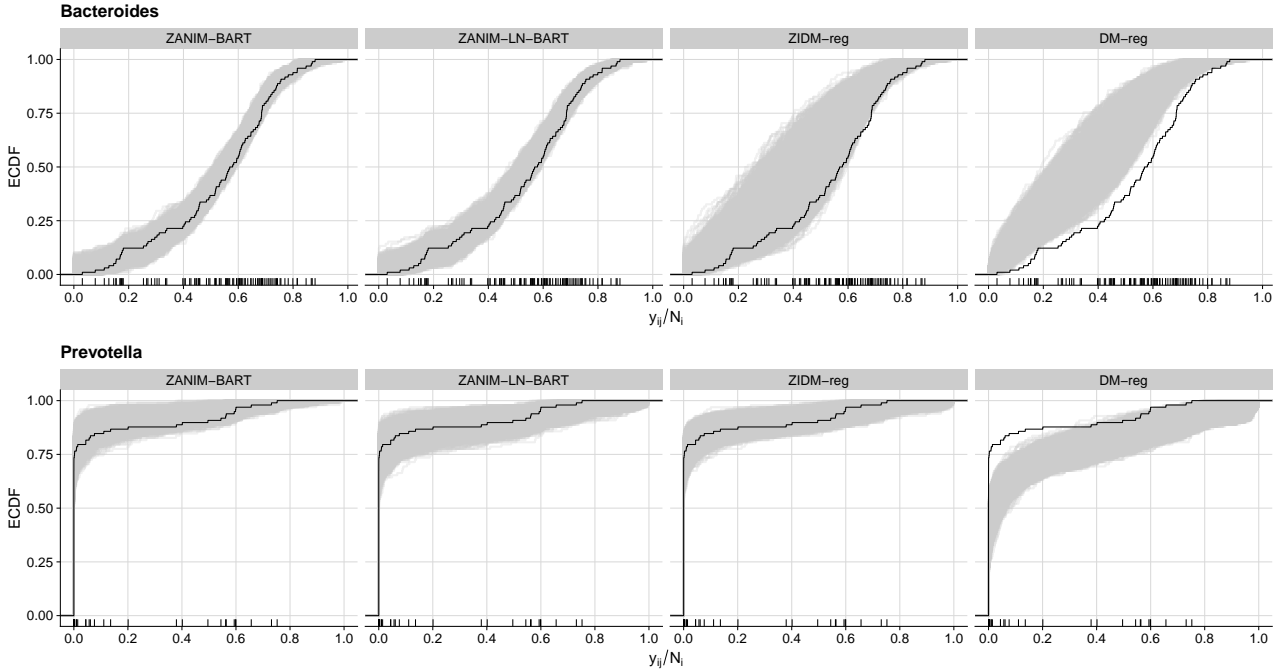


Fig. 4: Posterior predictive diagnostics for the ZANIM-BART, ZANIM-LN-BART, ZIDM-reg, and DM-reg models based on the marginal ECDF of the observed relative abundances, y_{ij}/N_i , for the *Bacteroides* and *Prevotella* taxa. The posterior predictive draws (grey lines) from the ZANIM-BART and ZANIM-LN-BART models closely follow the observed data (black lines), whereas the ZIDM-reg and DM-reg models fail to adequately capture the underlying patterns, particularly for the *Bacteroides* taxa. The rugs along the x -axes indicate the observed data.

the closed-form PMFs for the ZIDM and ZANIM distributions was derived in [Menezes et al. \(2025\)](#). The results in Table 2 are consistent with the posterior-predictive diagnostics and indicate that ZANIM-LN-BART model has the lowest WAIC, followed by the ZANIM-BART model. These results also suggest that ZANIM-LN-BART may be capturing additional overdispersion compared to the ZANIM-BART model, resulting in a better fit. For both the ZANIM-LN-BART and ZANIM-BART models, the estimated effective numbers of parameters, p_{waic} , are smaller than the competing ZIDM-reg and DM-reg models and substantially less than the actual number of parameters; a total of $d \times (m_\theta + m_\zeta) = 112,000$ regression trees and their associated terminal node parameters arising from the category-specific BART priors $f_j^{(c)}$ and $f_j^{(0)}$. This illustrates the strong effects of the regularised BART priors discussed in Section 2.5. The p_{waic} under the ZIDM-reg model is notably large compared with our models — nearly half the actual number of regression coefficients, $2 \times d \times (p + 1) = 5,488$ — and it is even larger under the DM-reg model. This suggests that although the spike-and-slab priors induce some sparsity, our models achieve this more effectively while also capturing nonlinear and interaction effects which cannot be obtained under restrictive parametric linear assumptions.

Table 2: Likelihood-based model comparison of the four models under consideration for the microbiome data, where p_{waic} is an estimate of the effective number of parameters and a lower WAIC value indicates a superior parsimonious fit.

Model	p_{waic}	WAIC
ZANIM-LN-BART	1,028.59	13,729.52
ZANIM-BART	1,086.69	13,974.57
ZIDM-reg	1,499.43	21,180.49
DM-reg	2,740.23	27,903.32

Given the improvement in fit, we might suspect that ZANIM-BART and ZANIM-LN-BART are identifying important dietary covariates and possibly nonlinear effects that the ZIDM-reg and DM-reg models are unable to capture. We thus compare the number of dietary covariates identified by the four models for each taxa.

Fig. 5 shows the marginal posterior probability of inclusion (MPPI) of the $d \times p = 2,716$ taxa/covariate pairs associated with the compositional and structural zero probabilities. Under ZANIM-BART and ZANIM-LN-BART, the MPPI is computed separately for the compositional and zero-inflation probabilities by averaging the number of times a covariate is used to define a splitting rule over all corresponding trees and iterations. Under ZIDM-reg and DM-reg, the MPPI for each taxa/covariate pair is obtained by averaging the respective inclusion indicators over the MCMC draws. Subject to the threshold of $\text{MPPI} \geq 0.5$ in Panel A of Fig. 5, we have that ZANIM-BART and ZANIM-LN-BART identify 323 and 287 taxa/covariate pairs, respectively, associated with the compositional probabilities. Among those, 243 and 146, respectively, have MPPI greater than 0.98, which corresponds to a Bayesian false discovery rate of 0.1. We would expect that ZANIM-BART would require more than ZANIM-LN-BART, since the latter captures additional unobserved variation, which helps to account for sampling zeros. In comparison, the ZIDM-reg and DM-reg models select 51 and 23 covariates, of which just 5 and 1, respectively, have MPPI values greater than 0.98. Regarding the structural zero probabilities, a similar analysis from Panel B of Fig. 5 indicates that ZANIM-BART and ZANIM-LN-BART identify 29 and 33 taxa/covariate pairs with MPPI greater than 0.5; among those, 7 for both models, have MPPI greater than 0.98. In contrast, ZIDM-reg only selects 5 covariates, none of which have MPPI greater than 0.98. Although our models identify a larger number of covariates than the ZIDM-reg and DM-reg models, these results together with the goodness-of-fit analyses above suggest that ZIDM-reg and DM-reg are potentially missing important covariates, leading to poor fits. It is also noteworthy from Panels A and B that the spike-and-slab prior of the ZIDM-reg and DM-reg models does not lead to exactly sparse variable selection in either case, since none of the taxa/covariate pairs on either level of either model have exactly zero MPPI values. Additional results in the Supplementary Material illustrate nonlinear dietary covariate effects on the compositional and structural zero probabilities that the ZANIM-LN-BART model are able to uncover.

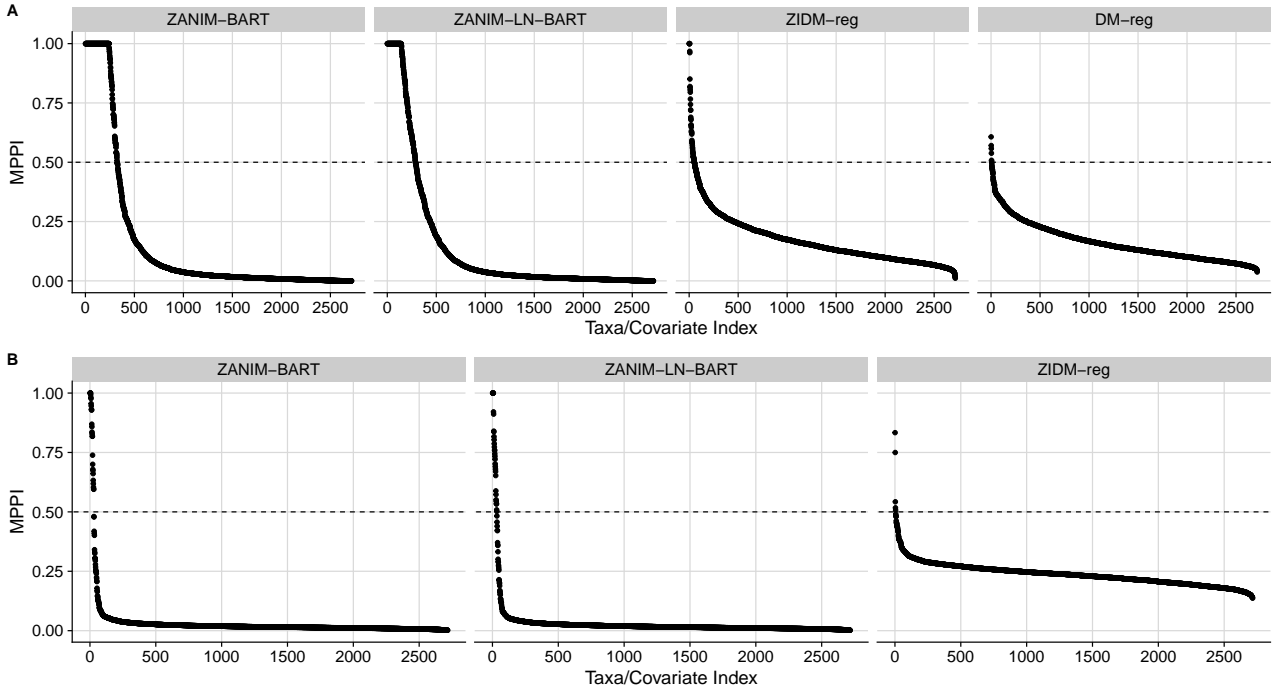


Fig. 5: Marginal posterior probability of inclusion (MPPI) of the $d \times p = 2,716$ taxa/covariate pairs associated with the population-level count (Panel A) and zero-inflation Panel B) probabilities, estimated using the ZANIM-BART, ZANIM-BART-LN, ZIDM-reg, and DM-reg models. The indices on the x -axes are sorted in ascending order of MPPI to facilitate comparison across the models.

4.2 Modern pollen-climate data

A key step in quantitative palaeoclimate reconstruction methods is to build a model to describe the relationships between the present vegetation and climatic drivers. Counts of pollen grains are commonly used to reflect the vegetation for a specific climate, such that changes in pollen composition provide information about the climate at that location. In this illustration, our goal is to showcase the benefits and flexibility of our ZANIM-BART and ZANIM-LN-BART models for modelling pollen-climate relationships. We consider an updated version of the data used by [Haslett et al. \(2006\)](#) and [Parnell et al. \(2015\)](#), containing $n = 7832$ samples of $d = 28$ pollen taxa collected at different locations in the Northern Hemisphere, along with three climate covariates: GDD5, the growing degree days above 5°C , calculated as the sum of daily temperatures above 5°C over a year; MTCO, the mean temperature of the coldest month in degrees Celsius; and AET/PET, the ratio of actual to potential evapotranspiration. The total counts, N_i , range from 74 to 1003 and there is a high degree of sparsity, with 63.21% of the counts being zero.

Previous studies suggested that the relationships between pollen composition and climate covariates are nonlinear (e.g., [Haslett et al., 2006](#); [Vasko et al., 2000](#)). We thus omit the ZIDM-reg model from the comparison due to its unrealistic parametric linear assumptions and address nonlinearities through the nonparametric BART priors of our proposed models, which obviate the need to pre-specify functional forms. We run the MCMC algorithms of the ZANIM-BART and ZANIM-LN-BART models for 10,000 iterations and discard the first 5,000 as burn-in. These settings took approximately 8 hours to run for both models. Given the size of the data, we consider this a reasonable computational time for models of such complexity with BART priors.

To assess goodness-of-fit and compare our two models, we leave out 2,000 samples at random and compute Bayesian diagnostics based on the marginal ECDFs of y_{ij}/N_i and the corresponding posterior-predictive distributions using this test set. [Fig. 6](#) gives these results for the four most abundant taxa: *Pinus.D* (Pine), *Gramineae* (true grasses), *Betula* (Birch), and *Picea* (Spruce). We observe that the posterior-predictive distributions under both models closely follow the observed out-of-sample data for the *Betula* and *Picea* taxa. However, ZANIM-BART is clearly inadequate in reproducing the out-of-sample counts of the *Pinus.D* and *Gramineae* taxa. Although we have empirical evidence of zero-inflation for both *Pinus.D* and *Gramineae*, the observed percentage of zeros are relatively small compared to other taxa — 10.26% for *Gramineae* and 6.66% for *Pinus.D*. This suggests that accounting for taxa-specific variations in the model is crucial and explains why ZANIM-LN-BART provides substantially better fit for these taxa compared to the ZANIM-BART model. The taxa-specific out-of-sample ranked probability scores reported in the Supplementary Material provide further evidence that ZANIM-LN-BART is more effective at describing the data than ZANIM-BART.

We conclude this analysis by illustrating the marginal effects that the climate covariates GDD5, MTCO, and AET/PET have on the compositional and structural zero probabilities under ZANIM-LN-BART using partial dependence plots (PDPs; [Friedman, 2001](#)). To do so, we create a three-dimensional grid which represents the observed climate sites, following the approach of [Haslett et al. \(2006\)](#). This yields 3120 observations, where each of the three covariates have 31 unique values. From these PDPs, researchers can obtain insights on how the climate conditions affect both the abundance and absence of pollen taxa. [Fig. 7](#) shows the PDPs for *Picea* and *Pinus.D*, with one panel per covariate. The PDPs for the compositional probabilities (blue curves) effectively smooth the observed compositions (black points) and the structural zero probabilities (orange curves) are consistent with the observed zeros (orange rugs). Overall, it is apparent that ZANIM-LN-BART aids to prevent biased estimation of the covariate effects, such as downward (upward) bias under zero-inflation (N -inflation), and enables the identification of climatic regions with high or low structural zero probabilities.

We observe a unimodal climate response of *Picea* to GDD5 in Panel **B**, with a mode around 1000. As GDD5 increases beyond this value, the compositional and structural zero probabilities decrease and increase, respectively. Consistent with the observed zeros indicated by the rug, this suggests that *Picea* is less likely to be observed under warmer growing conditions. In Panel **B**, MTCO exhibits a quadratic effect on the structural zero probabilities for *Picea*, with higher probabilities under extremely cold and hot conditions ($\text{MTCO} < 30^{\circ}\text{C}$ and $\text{MTCO} > 20^{\circ}\text{C}$), and the effect on the compositional probabilities is again unimodal, with the mode being

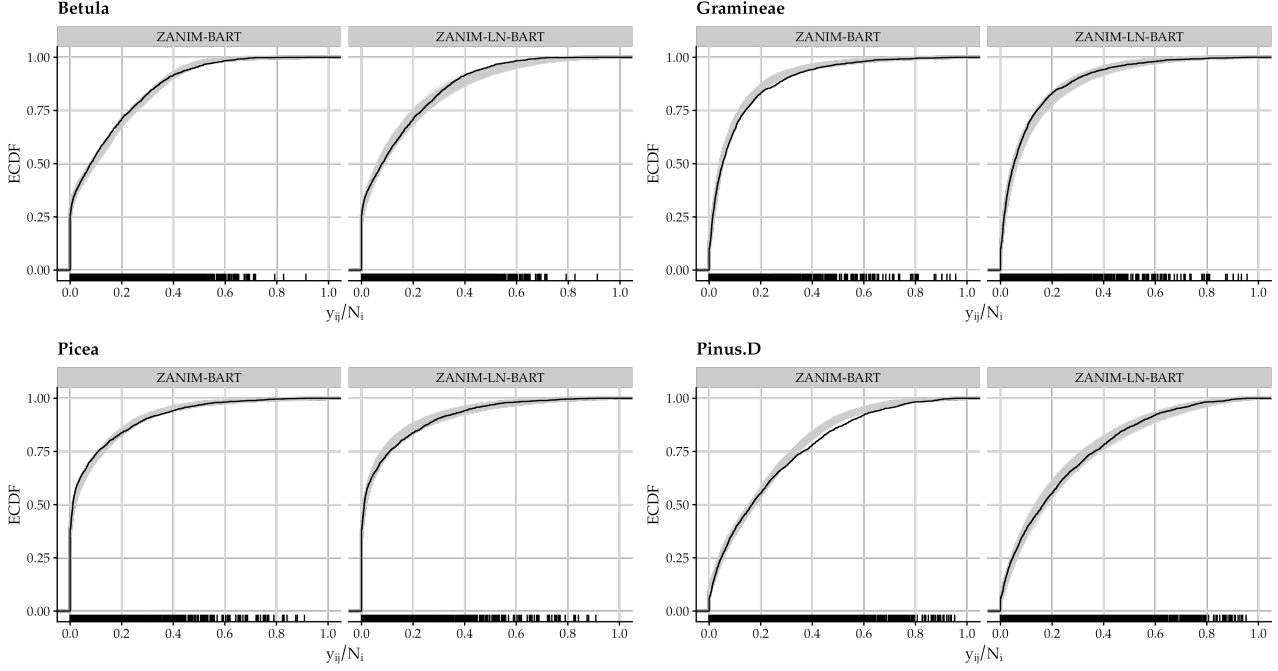


Fig. 6: Out-of-sample posterior predictive diagnostics for the ZANIM-BART and ZANIM-LN-BART models based on the marginal ECDFs of the observed relative abundances, y_{ij}/N_i , for the four most abundant pollen taxa. The rugs along the x -axes indicate the observed data.

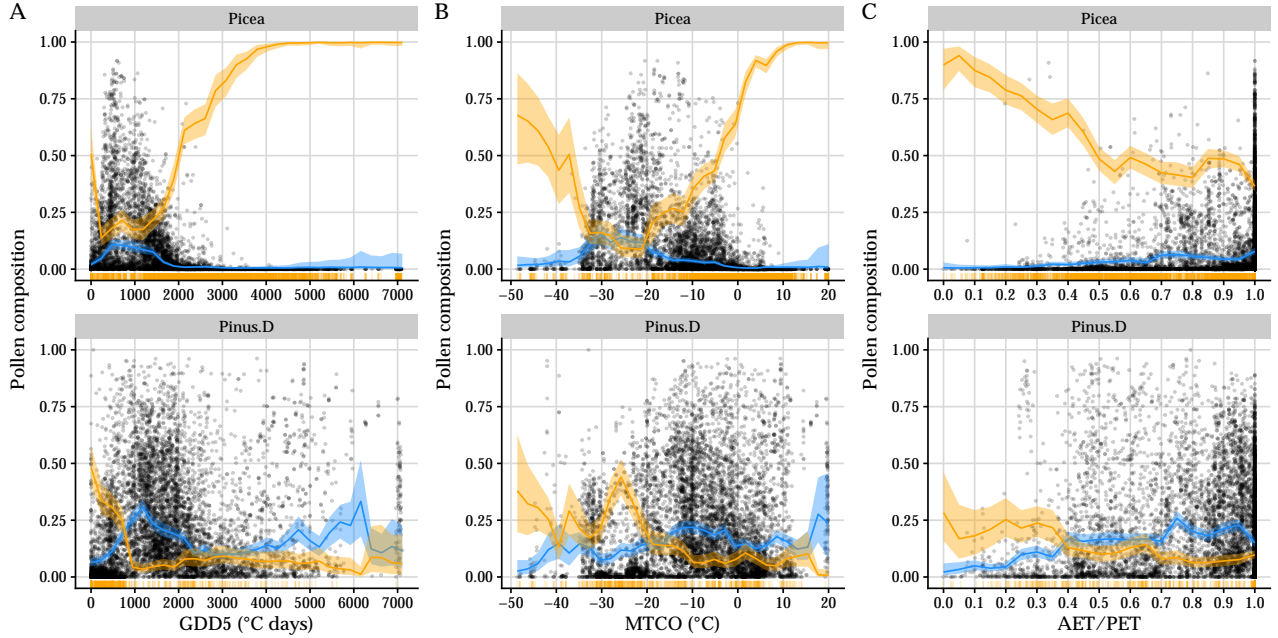


Fig. 7: Partial dependence plots (PDPs) of the climate covariate effects for *Picea* and *Pinus.D*. Black dots represent the observed relative abundances, y_{ij}/N_i , and the orange rugs along the x -axes represent samples where the observed counts are zero. These PDPs show the effects of the climate covariates GDD5 (growing season warmth, Panel A), MTCO (harshness of winter, Panel B), and AET/PET (available moisture, Panel C), on the population-level count (blue) and structural zero probabilities (orange) via superimposed curves, along with associated 95% credible interval bands.

between -30 and -20 . Finally, regarding the PDPs for AET/PET and *Picea* shown in Panel C, we see a nearly constant linear effect on the compositional probabilities with small peaks around AET/PET values between 0.7 and 0.9 , with a further linear negative effect on the structural zero probabilities.

On the other hand, for *Pinus.D*, we observe a multimodal effect of GDD5 on the compositional probabilities, with two notable modes around 1000 and 6000 , where the latter displays large uncertainty due to the scarcity

of observations with GDD5 around 6000 (see Panel **A**). The probability of structural zeros is elevated when GDD5 is nearly 0, but the effect is insubstantial and largely flat at higher GDD5 values. Similarly, Panels **B** and **C** indicate multimodal effects of MTCO and AET/PET on the compositional probabilities and modest (though still nonlinear) effects on the structural zero probabilities for *Pinus.D*. As the estimated zero-inflation probabilities are much smaller than those for *Picea*, this suggests that the observed zeros in *Pinus.D* are primarily explained by unobserved heterogeneity captured through the random effects in the ZANIM-LN-BART model, rather than direct climatic influences. This interpretation is consistent with the superior posterior predictive performance of the ZANIM-LN-BART model relative to the ZANIM-BART model for this taxon (see Fig. 6).

5 Discussion

Our novel ZANIM-BART and ZANIM-LN-BART models represent advances over existing approaches for modelling count-compositional data by simultaneously addressing key challenges commonly encountered in such data, including an excess of zeros, overdispersion, and cross-sample heterogeneity, while flexibly modelling covariate effects without relying on restrictive parametric linear assumptions. This is achieved by extending the ZANIM distribution (Menezes et al., 2025) with independent nonparametric log-linear BART and probit-BART priors on the category-specific parameters that relate the covariates to both the compositional and structural zero probabilities, respectively. Our ZANIM-LN-BART model further incorporates log-linear multivariate Gaussian random effects, which allows for excess variation to be explained by unobserved latent characteristics and captures complex dependence among the categories.

We developed an efficient MCMC algorithm for conducting inference for both proposed models and demonstrated its efficacy through simulation studies. We combine the data augmentation schemes introduced by Menezes et al. (2025) for the ZANIM distribution with the established BART sampling routines of Chipman et al. (2010) and Murray (2021). Conceptually, our models extend the multinomial-logistic BART framework of Murray (2021) in two directions: ZANIM-BART introduces category-specific BART priors to accommodate excess zeros and ZANIM-LN-BART model further generalises this by incorporating latent random effects to account for unobserved heterogeneity. We provide an efficient C++ implementation of our models via the R package `zanicc` available from the repository at <https://github.com/AndrMenezes/zanicc>.

Our simulation studies also demonstrated the benefits of including the BART priors in our models when the goal is to estimate unknown complex covariate effects, improving existing models such as the ZIDM regression model which assumes linear functional forms. We further illustrated our models through analyses of data from microbiome and palynology experiments. In the analysis of a benchmark human gut microbiome data set, we showed that ZANIM-BART and ZANIM-LN-BART provide superior fits than the alternative ZIDM and DM regression models, while also being able to identify important covariates when the sparsity-inducing Dirichlet prior of Linero (2018) is employed. For the palynology application, we presented valuable inferential outputs obtained from the ZANIM-LN-BART model which can help researchers to extract meaningful insights from their pollen count-compositional data. In particular, we discussed the effects of climate covariates on the pollen composition and identified climate conditions that can affect both the compositional and structural zero probabilities among the pollen taxa.

A general assumption of our proposed models is that the zero-inflation indicators, \mathbf{z}_i , are independent across the categories. This may be unrealistic in applied settings such as microbiome studies, where zeros may co-occur in two or more taxa, indicating that certain taxa tend to drop out together. To relax this assumption, while retaining category-specific BART priors for the structural zero probabilities, we intend to explore the introduction of shared Gaussian latent factors for \mathbf{z}_i within the nonparametric seemingly unrelated probit BART framework of Esser et al. (2025). This extension would require only minor modifications in the updates of the regression trees parameters associated with the structural zero probabilities, along with an additional sampling step for the correlation matrix of the shared Gaussian random effects. The use of shared latent factors

would be analogous to the Gaussian random effects presently used in the ZANIM-LN-BART model to capture dependence and overdispersion.

It is also of interest to reduce the computational cost of our models associated to the large total number of regression trees, $d \times (m_\theta + m_\zeta)$, while maintaining the flexibility of the BART priors. A research direction in this line is to consider the shared trees framework of [Linero et al. \(2020\)](#). In this approach, the tree structure could be shared within each category by using the same tree topology for the compositional and zero- inflation probabilities, or shared across the categories for both sets of parameters. Preliminary experiments in a high- d setting indicate that the computational speed of our models is greatly improved when adopting a shared trees approach, at the expense of only a minor loss of performance relative to the ZANIM-BART and ZANIM-LN-BART models. We intend to further investigate this approach in future work.

Lastly, we would also like to incorporate the ZANIM-BART and ZANIM-LN-BART models into the complete palaeoclimate reconstruction framework of [Parnell et al. \(2015\)](#). However, this would require an extension to overcome BART’s inherent lack of smoothness, as smoothness is typically assumed for the climate-space induced by the covariates ([Haslett et al., 2006](#); [Vasko et al., 2000](#)). The soft-BART of [Linero and Yang \(2018\)](#) and the GP-BART of [Maia et al. \(2024\)](#) are approaches that can be leveraged to enforce such smoothness, though both would add considerable computational cost.

Overall, we envisage that our proposed models will be particularly valuable in zero-inflated count-compositional settings where the goal is to uncover complex covariate effects on both the count and structural zero components, while simultaneously accounting for high degrees of overdispersion and complex dependencies among the categories.

Acknowledgments

André F. B. Menezes’s work was supported by Taighde Éireann – Research Ireland under Grant number 18/CRT/6049. Andrew Parnell’s work was additionally supported by: the UCD-Met Éireann Research Professorship Programme (28-UCDNWPAI); Northern Ireland’s Department of Agriculture, Environment and Rural Affairs (DAERA), UK Research and Innovation (UKRI) via the International Science Partnerships Fund (ISPF) under Grant number [22/CC/11103] at the Co-Centre for Climate + Biodiversity + Water; Decarb-AI, supported by AIB and Research Ireland: an Innovate for Ireland Centre (25/I4I-TC/13542); and a Research Ireland award (12/RC/2289_P2).

References

Albert, J. H. and Chib, S. (1993). “Bayesian analysis of binary and polychotomous response data.” *Journal of the American Statistical Association*, 88(422): 669–679.

Anderson, T. W. and Rubin, H. (1956). “Statistical Inference in Factor Analysis.” In Neyman, J. (ed.), *Proceedings of the Third Berkeley Symposium on Mathematical Statistics and Probability, Volume 5: Contributions to Econometrics, Industrial Research, and Psychometry*, 111–150. Berkeley, CA, USA: University of California Press. Symposium held at the Statistical Laboratory, University of California, Berkeley; December 26–31, 1954 and July–August, 1955.

Ascari, R., Migliorati, S., and Ongaro, A. (2025). “A new Dirichlet-multinomial mixture regression model for the analysis of microbiome data.” *Statistics in Medicine*, 44(18-19): e70220.

Bhattacharya, A. and Dunson, D. B. (2011). “Sparse Bayesian infinite factor models.” *Biometrika*, 98(2): 291–306.

Blasco-Moreno, A., Pérez-Casany, M., Puig, P., Morante, M., and Castells, E. (2019). “What does a zero mean? Understanding false, random and structural zeros in ecology.” *Methods in Ecology and Evolution*, 10(7): 949–959.

Bleich, J., Kapelner, A., George, E. I., and Jensen, S. T. (2014). “Variable selection for BART: An application to gene regulation.” *The Annals of Applied Statistics*, 8(3): 1750–1781.

Chen, J. and Li, H. (2013). “Variable selection for sparse Dirichlet-multinomial regression with an application to microbiome data analysis.” *Annals of Applied Statistics*, 7(1): 418–442.

Chipman, H. A., George, E. I., and McCulloch, R. E. (1998). “Bayesian CART model search.” *Journal of the American Statistical Association*, 93(443): 935–948.

— (2010). “BART: Bayesian additive regression trees.” *The Annals of Applied Statistics*, 4(1): 266–298.

Eddelbuettel, D. (2013). *Seamless R and C++ Integration with Rcpp*. New York: Springer. ISBN 978-1-4614-6867-7.

Esser, J., Maia, M. M., Parnell, A. C., Bosmans, J., van Dongen, H., Klausch, T., and Murphy, K. (2025). “Seemingly unrelated Bayesian additive regression trees for cost-effectiveness analyses in healthcare.” *The Annals of Applied Statistics*, 19(4): 3113–3140.

Friedman, J. H. (2001). “Greedy function approximation: A gradient boosting machine.” *The Annals of Statistics*, 29(5): 1189–1232.

Grantham, N. S., Guan, Y., Reich, B. J., Borer, E. T., and Gross, K. (2020). “MIMIX: A Bayesian mixed-effects model for microbiome data from designed experiments.” *Journal of the American Statistical Association*, 115(530): 599–609.

Haslett, J., Whiley, M., Bhattacharya, S., Salter-Townshend, M., Wilson, S. P., Allen, J. R. M., Huntley, B., and Mitchell, F. J. G. (2006). “Bayesian palaeoclimate reconstruction.” *Journal of the Royal Statistical Society. Series A (Statistics in Society)*, 169(3): 395–438.

Hastie, T. and Tibshirani, R. (2000). “Bayesian backfitting.” *Statistical Science*, 15(3): 196–213.

Kapelner, A. and Bleich, J. (2016). “bartMachine: Machine learning with Bayesian additive regression trees.” *Journal of Statistical Software*, 70(4): 1–40.

Koslovsky, M. D. (2023). “A Bayesian zero-inflated Dirichlet-multinomial regression model for multivariate compositional count data.” *Biometrics*, 79(4): 3239–3251.

Linero, A. R. (2017). “A review of tree-based Bayesian methods.” *Communications for Statistical Applications and Methods*, 24(6): 543–559.

— (2018). “Bayesian regression trees for high-dimensional prediction and variable selection.” *Journal of the American Statistical Association*, 113(522): 626–636.

Linero, A. R., Sinha, D., and Lipsitz, S. R. (2020). “Semiparametric mixed-scale models using shared Bayesian forests.” *Biometrics*, 76(1): 131–144.

Linero, A. R. and Yang, Y. (2018). “Bayesian regression tree ensembles that adapt to smoothness and sparsity.” *Journal of the Royal Statistical Society Series B: Statistical Methodology*, 80(5): 1087–1110.

Maia, M. M., Murphy, K., and Parnell, A. C. (2024). “GP-BART: A novel Bayesian additive regression trees approach using Gaussian processes.” *Computational Statistics & Data Analysis*, 190: 107858.

Menezes, A. F., Parnell, A. C., and Murphy, K. (2025). “Finite mixture representations of zero-and- N -inflated distributions for count-compositional data.” *Journal of Multivariate Analysis*, 210: 105492.

Mosimann, J. E. (1962). “On the compound multinomial distribution, the multivariate β -distribution, and correlations among proportions.” *Biometrika*, 49(1/2): 65–82.

Murphy, A. H. (1970). "The ranked probability score and the probability score: A comparison." *Monthly Weather Review*, 98(12): 917–924.

Murphy, K., Viroli, C., and Gormley, I. C. (2020). "Infinite mixtures of infinite factor analysers." *Bayesian Analysis*, 15(3): 937–963.

Murray, I., Adams, R., and MacKay, D. (2010). "Elliptical slice sampling." In Teh, Y. W. and Titterington, M. (eds.), *Proceedings of the Thirteenth International Conference on Artificial Intelligence and Statistics*, volume 9 of *Proceedings of Machine Learning Research*, 541–548. Chia Laguna Resort, Sardinia, Italy: PMLR.

Murray, J. S. (2021). "Log-linear Bayesian additive regression trees for multinomial logistic and count regression models." *Journal of the American Statistical Association*, 116(534): 756–769.

Parnell, A. C., Sweeney, J., Doan, T. K., Salter-Townshend, M., Allen, J. R. M., Huntley, B., and Haslett, J. (2015). "Bayesian inference for palaeoclimate with time uncertainty and stochastic volatility." *Journal of the Royal Statistical Society. Series C (Applied Statistics)*, 64(1): 115–138.

Ren, B., Bacallado, S., Favaro, S., Holmes, S., and Trippa, L. (2017). "Bayesian nonparametric ordination for the analysis of microbial communities." *Journal of the American Statistical Association*, 112(520): 1430–1442.

Ren, B., Bacallado, S., Favaro, S., Vatanen, T., Huttenhower, C., and Trippa, L. (2020). "Bayesian mixed effects models for zero-inflated compositions in microbiome data analysis." *The Annals of Applied Statistics*, 14(1): 494–517.

Ročková, V. and van der Pas, S. (2020). "Posterior concentration for Bayesian regression trees and forests." *The Annals of Statistics*, 48(4): pp. 2108–2131.

Rue, H. and Held, L. (2005). *Gaussian Markov Random Fields: Theory and Applications*, volume 104 of *Monographs on Statistics and Applied Probability*. London, UK: Chapman and Hall/CRC Press.

Rue, H., Martino, S., and Chopin, N. (2009). "Approximate Bayesian inference for latent Gaussian models by using integrated nested Laplace approximations." *Journal of the Royal Statistical Society: Series B (Statistical Methodology)*, 71(2): 319–392.

Salter-Townshend, M. and Haslett, J. (2012). "Fast inversion of a flexible regression model for multivariate pollen counts data." *Environmetrics*, 23: 595–605.

Sparapani, R., Spanbauer, C., and McCulloch, R. (2021). "Nonparametric machine learning and efficient computation with Bayesian additive regression trees: The BART R Package." *Journal of Statistical Software*, 97(1): 1–66.

Sparapani, R. A., Logan, B. R., Maiers, M. J., Laud, P. W., and McCulloch, R. E. (2023). "Nonparametric failure time: Time-to-event machine learning with heteroskedastic Bayesian additive regression trees and low information omnibus Dirichlet process mixtures." *Biometrics*, 79(4): 3023–3037.

Sweeney, J. (2012). "Advances in Bayesian Model Development and Inversion in Multivariate Inverse Inference Problems with Application to Palaeoclimate Reconstruction." Ph.D. thesis, Trinity College Dublin.

Tang, Z.-Z. and Chen, G. (2019). "Zero-inflated generalized Dirichlet multinomial regression model for microbiome compositional data analysis." *Biostatistics*, 20(4): 698–713.

Tipton, J. R., Hootem, M. B., Nolan, C., Booth, R. K., and McLachlan, J. (2019). "Predicting paleoclimate from compositional data using multivariate Gaussian process inverse prediction." *The Annals of Applied Statistics*, 13(4): 2363–2388.

Urbas, S., Lovera, P., Daly, R., O'Riordan, A., Berry, D., and Gormley, I. C. (2024). “Predicting milk traits from spectral data using Bayesian probabilistic partial least squares regression.” *The Annals of Applied Statistics*, 18(4): 3486–3506.

Vasko, K., Toivonen, H., and Korhola, A. (2000). “A Bayesian multinomial Gaussian response model for organism-based environmental reconstruction.” *Journal of Paleolimnology*, 24: 243–250.

Wadsworth, D. W. (2017). “An integrative Bayesian Dirichlet-multinomial regression model for the analysis of taxonomic abundances in microbiome data.” *BMC Bioinformatics*, 18(94).

Watanabe, S. (2010). “Asymptotic equivalence of Bayes cross validation and widely applicable information criterion in singular learning theory.” *Journal of Machine Learning Research*, 11: 3571–3594.

Wood, S. N. (2017). *Generalized Additive Models: An Introduction with R*. Chapman and Hall/CRC, 2nd edition.

Woody, S., Carvalho, C. M., and Murray, J. S. (2021). “Model interpretation through lower-dimensional posterior summarization.” *Journal of Computational and Graphical Statistics*, 30(1): 144–161.

Wu, G., Chen, J., Hoffmann, C., Bittinger, K., Chen, Y.-Y., Keilbaugh, S., Bewtra, M., Knights, D., W.A., W., Knight, R., Sinha, R., Gilroy, E., Gupta, K., Baldassano, R., Nessel, L., Li, H., Bushman, F., and Lewis, J. (2011). “Linking long-term dietary patterns with gut microbial enterotypes.” *Science*, 334(6052): 105–108.

Xia, F., Chen, J., Fung, W. K., and Li, H. (2013). “A logistic normal multinomial regression model for microbiome compositional data analysis.” *Biometrics*, 69(4): 1053–1063.

Zeng, Y., Pang, D., Zhao, H., and Wang, T. (2023). “A zero-inflated logistic normal multinomial model for extracting microbial compositions.” *Journal of the American Statistical Association*, 118(544): 2356–2369.

Supplementary Material

The Supplementary Material includes further details on the ZANIM-LN distribution in Section S.1, derivations for the data augmentations and posterior inference scheme for the ZANIM-LN-BART model in Section S.2, and additional results for the simulation studies (Section S.3) and the two case studies presented in the main paper (Section S.4 and Section S.5, for the human gut microbiome and modern pollen-climate data analyses, respectively).

S.1 Additional details on the ZANIM-LN distribution

Section 2.1 introduced the ZANIM-LN distribution by incorporating subject-specific random effects on the compositional probabilities of the ZANIM distribution. Here, we compare the theoretical properties of the ZANIM-LN distribution in relation to the ZANIM and ZANIDM distributions. We follow Menezes et al. (2025) and present marginal PMF plots and theoretical moments for an example with $d = 3$ categories and $N = 30$ trials. We use similar parameter values as per Menezes et al. (2025) for the ZANIM and ZANIDM distributions with common zero-inflation parameters and expectations given by $\zeta = (0.05, 0.15, 0.10)$ and $\mathbb{E}[\mathbf{Y}] = (2.320, 18.496, 9.161)$, respectively. For the ZANIM-LN distribution, we specify the covariance matrix of the random effects as

$$\boldsymbol{\Sigma} = \begin{pmatrix} 0.5 & -0.4 & 0.1 \\ -0.4 & 0.6 & 0.3 \\ 0.1 & 0.3 & 0.7 \end{pmatrix},$$

and set its concentration parameters as $\boldsymbol{\alpha} \in \{0.031, 0.770, 0.241\}$, in order to match the same expectations. We remind the reader that the ZANIM-LN distribution does not have a closed-form expression for its PMF. However, we can approximate it using Monte Carlo simulation; in particular, we generate $\mathbf{u}_i \sim \text{Normal}_3[\mathbf{0}_3, \boldsymbol{\Sigma}]$ $i = 1, \dots, 5000$ random samples and evaluate the analytical expression of the marginal PMF of the ZANIM distribution, for each category $j \in \{1, \dots, d = 3\}$, conditional on $\theta_{ij} = \alpha_j e^{u_{ij}} / \sum_{k=1}^d \alpha_k e^{u_{ik}}$ and $\zeta \in \{0.05, 0.15, 0.10\}$, then average it to obtain the marginal PMFs under the ZANIM-LN distribution.

The marginal PMFs plots are given in Fig. S.1. We clearly see that the ZANIM-LN distribution maintains the zero- and N -inflation characteristics while accommodating more overdispersed counts than the ZANIM and ZANIDM distributions. In the first marginal, Y_1 , we observe a large spike at $k = 0$, under all three distributions, which consists not only of structural zeros, but also many sampling zeros. Interestingly, this spike is large in the ZANIM-LN distribution, suggesting that it is capable of accounting for zeros due to overdispersion. The second marginal, Y_2 , illustrates the large presence of structural zeros for all three distributions, which is expected given that $\zeta_3 = 0.15$. It is also evident how the ZANIM-LN distribution is more overdispersed than its counterparts. Finally, the multimodality evident in the plots of the third marginal, Y_3 , shows the finite mixture nature of all three distributions. We can also clearly see that ZANIM-LN distribution has a heavy right tail consistent with the high degree of overdispersion.

A similar Monte Carlo approximation using the laws of iterated expectations and variances was employed to obtain the moments of the ZANIM-LN distribution. In Table S.1, we compare the theoretical means and variances under ZANIM, ZANIDM, and ZANIM-LN for the above $d = 3$ setting. We also include the theoretical dispersion index, $\text{DI}[Y_j] = \text{Var}[Y_j]/\mathbb{E}[Y_j]$, and the following zero-inflation index:

$$\text{ZI}_b[Y_j] = 1 + (\text{Var}[Y_j] - \mathbb{E}[Y_j]) \frac{\log \Pr[Y_j = 0]}{\mathbb{E}^2[Y_j] \log \text{DI}[Y_j]},$$

which was proposed by Blasco-Moreno et al. (2019). Note that $\text{ZI}_b[Y_j]$ takes into account the empirical variance and the dispersion index, so it measures the extent to which the zeros can be explained by the overdispersion. In addition, when the marginal distribution of Y_j follows a binomial or negative-binomial distribution, then $\text{ZI}_b[Y_j] = 0$, indicating no zero-inflation, while when $\text{ZI}_b > 0$, we have evidence of zero-inflation that cannot be described only by the overdispersion. Consistent with the PMF plots from Fig. S.1, we can see that ZANIM-LN

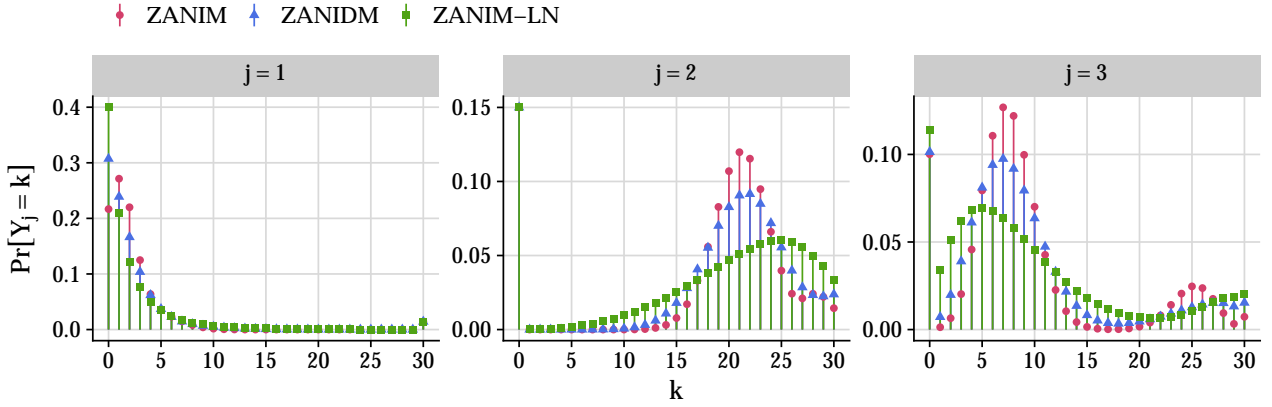


Fig. S.1: Comparison of the marginal PMFs of ZANIM (red circles), ZANIDM (blue triangles), and ZANIM-LN (green squares), with $\theta \in \{0.05, 0.70, 0.25\}$ for ZANIM, $\alpha \in \{2.0, 28.0, 10.0\}$ for ZANIDM, and $\alpha \in \{0.031, 0.770, 0.241\}$ for ZANIM-LN, along with the category-specific probabilities of structural zeros $\zeta \in \{0.05, 0.15, 0.10\}$ and $N = 30$ trials in each case. These parameter settings ensure that all three distributions have the same expectations, with $\mathbb{E}[\mathbf{Y}] = (2.320, 18.496, 9.161)$.

has the largest variance in all three marginals, highlighting its greater flexibility in modelling overdispersion. It is interesting to note that $ZI_b[Y_1] < 0$, suggesting that zero-inflation in this marginal could be explained by the finite mixture nature of the distribution and its ability to capture overdispersion, which is consistent with the low values for the structural zero probability $\zeta_1 = 0.05$ and also for the count probability parameters: $\theta_1 = 0.05$ for ZANIM, $\alpha_1 = 2.0$ for ZANIDM, and $\alpha_1 = 0.031$ for ZANIM-LN. In contrast, for the second and third marginals, the fact that $ZI_b[Y_j] > 0$ shows the ability of the models to handle structural zeros.

Table S.1: Comparison of the theoretical moments of ZANIM, ZANIDM, and ZANIM-LN distributions, with $\theta \in \{0.05, 0.70, 0.25\}$ for ZANIM, $\alpha \in \{2.0, 28.0, 10.0\}$ for ZANIDM, and $\alpha \in \{0.031, 0.770, 0.241\}$ for ZANIM-LN, along with $\zeta \in \{0.05, 0.15, 0.10\}$ and $N = 30$ trials in each case. These parameter settings ensure that all three distributions have the same expectations, i.e., $\mathbb{E}[\mathbf{Y}] = (2.320, 18.496, 9.161)$.

	Distribution	$\mathbb{E}[Y_j]$	$\text{Var}[Y_j]$	$\text{DI}[Y_j]$	$ZI_b[Y_j]$
$j = 1$	ZANIM	2.320	14.326	6.174	-0.873
	ZANIDM	2.320	16.392	7.064	-0.577
	ZANIM-LN	2.320	19.002	8.189	-0.351
$j = 2$	ZANIM	18.496	69.178	3.740	0.787
	ZANIDM	18.496	72.723	3.932	0.780
	ZANIM-LN	18.496	86.981	4.703	0.755
$j = 3$	ZANIM	9.161	50.409	5.502	0.337
	ZANIDM	9.161	54.658	5.966	0.305
	ZANIM-LN	9.161	65.776	7.180	0.258

S.2 Additional details on the inference for the ZANIM-LN-BART model

Following the notation of the main paper where $f_j^{(c)}(\mathbf{x}_i)$ and $f_j^{(0)}(\mathbf{x}_i)$ are the category-specific BART priors for the population-level count and structural zero probabilities given in (3) and (4), respectively, we can thus define the ZANIM-LN-BART model through the following stochastic representation:

$$\begin{aligned} (z_{ij} \mid f_j^{(0)}(\mathbf{x}_i)) &\stackrel{\text{ind.}}{\sim} \text{Bernoulli} \left[1 - \Phi \left(f_j^{(0)}(\mathbf{x}_i) \right) \right], \quad j \in \{1, \dots, d\}, \\ \mathbf{v}_i &\sim \text{Normal}_{d-1} [\mathbf{0}_{d-1}, \boldsymbol{\Sigma}_V], \end{aligned}$$

$$\begin{aligned}\vartheta_{ij} &= \frac{z_{ij} f_j^{(c)}(\mathbf{x}_i) e^{u_{ij}}}{\sum_{k=1}^d z_{ik} f_k^{(c)}(\mathbf{x}_i) e^{u_{ik}}}, \quad j \in \{1, \dots, d\}, \\ (\mathbf{Y}_i \mid N_i, \vartheta_i) &\sim \begin{cases} \delta_{\mathbf{0}_d}(\cdot), & \text{if } z_{ij} = 0 \forall j \in \{1, \dots, d\}, \\ \text{Multinomial}_d[N_i, \vartheta_{i1}, \dots, \vartheta_{id}], & \text{otherwise,} \end{cases}\end{aligned}\quad (\text{S.13})$$

where $\mathbf{u}_i = \mathbf{B}\mathbf{v}_i$, and $\mathbf{B} \in \mathbb{R}^{d \times (d-1)}$ is an orthogonal matrix, such that $\sum_{j=1}^d u_{ij} = 0$. Setting $\mathbf{u}_i = \mathbf{0}_d$ leads to the ZANIM-BART model.

S.2.1 Augmented likelihood

Combining the stochastic representation of the ZANIM-LN-BART model given in (S.13) with the data augmentation in (5), we can derive the following augmented likelihood contribution for the i -th observation:

$$\begin{aligned}\mathcal{L}_i &\propto \prod_{j=1}^d \left\{ \left[\Phi(f_j^{(0)}(\mathbf{x}_i)) \right]^{1-z_{ij}} \left[1 - \Phi(f_j^{(0)}(\mathbf{x}_i)) \right]^{z_{ij}} \left[\frac{z_{ij} f_j^{(c)}(\mathbf{x}_i) e^{u_{ij}}}{\sum_{k=1}^d z_{ik} f_k^{(c)}(\mathbf{x}_i) e^{u_{ik}}} \right]^{y_{ij}} \right\} \\ &\quad \times \left[\sum_{j=1}^d z_{ij} f_j^{(c)}(\mathbf{x}_i) e^{u_{ij}} \right]^{N_i} \exp \left[-\phi_i \sum_{j=1}^d z_{ij} f_j^{(c)}(\mathbf{x}_i) e^{u_{ij}} \right] \\ &\propto \prod_{j=1}^d \left\{ \left[\Phi(f_j^{(0)}(\mathbf{x}_i)) \right]^{1-z_{ij}} \left[1 - \Phi(f_j^{(0)}(\mathbf{x}_i)) \right]^{z_{ij}} \left[z_{ij} f_j^{(c)}(\mathbf{x}_i) e^{u_{ij}} \right]^{y_{ij}} \right\} \\ &\quad \times \exp \left[-\phi_i \sum_{j=1}^d z_{ij} f_j^{(c)}(\mathbf{x}_i) e^{u_{ij}} \right] \\ &\propto \prod_{j=1}^d \left\{ \left[\Phi(f_j^{(0)}(\mathbf{x}_i)) \right]^{1-z_{ij}} \left[1 - \Phi(f_j^{(0)}(\mathbf{x}_i)) \right]^{z_{ij}} \left[z_{ij} f_j^{(c)}(\mathbf{x}_i) \right]^{y_{ij}} e^{-\phi_i z_{ij} f_j^{(c)}(\mathbf{x}_i) e^{u_{ij}}} \right\} \\ &\propto \prod_{j=1}^d \left\{ \left[\Phi(f_j^{(0)}(\mathbf{x}_i)) \right]^{1-z_{ij}} \left[1 - \Phi(f_j^{(0)}(\mathbf{x}_i)) \right]^{z_{ij}} \left[f_j^{(c)}(\mathbf{x}_i) \right]^{y_{ij}} e^{-\phi_i z_{ij} f_j^{(c)}(\mathbf{x}_i) e^{u_{ij}}} \right\},\end{aligned}$$

where we can drop the term z_{ij} multiplying $f_j^{(c)}(\mathbf{x}_i)$ in the third expression because $z_{ij} = 1$ when $y_{ij} > 0$ by construction. Evaluating the terms \mathcal{L}_i across all n observations yields the augmented likelihood in (6).

Obviously, we have that $z_{ij} = 1$ when $y_{ij} > 0$. On the other hand, the full conditional distribution of $z_{ij} \in \{0, 1\}$ given the observed data and the parameters when $y_{ij} = 0$ is

$$p(z_{ij} = 0 \mid y_{ij} = 0, \dots) \propto \Phi(f_j^{(0)}(\mathbf{x}_i)),$$

and

$$p(z_{ij} = 1 \mid y_{ij} = 0, \dots) \propto \left[1 - \Phi(f_j^{(0)}(\mathbf{x}_i)) \right] e^{-\phi_i z_{ij} f_j^{(c)}(\mathbf{x}_i) e^{u_{ij}}}.$$

By normalising the above probabilities, we obtain the full conditional given in (8).

Finally, to obtain the further augmented likelihood in (7), we apply the data augmentation approach of [Albert and Chib \(1993\)](#) to (6). We have that the conditional distribution of w_{ij} given z_{ij} is a truncated normal distribution with probability density function given by

$$p(w_{ij} \mid z_{ij}) = \left[\frac{\varphi(w_{ij}; f_j^{(0)}(\mathbf{x}_i), 1)}{1 - \Phi(f_0^{(j)}(\mathbf{x}_i))} \right]^{z_{ij}} \left[\frac{\varphi(w_{ij}; f_j^{(0)}(\mathbf{x}_i), 1)}{\Phi(f_0^{(j)}(\mathbf{x}_i))} \right]^{1-z_{ij}}.$$

Then, the augmented likelihood for the zero-inflation BART component of category j takes the form

$$p(w_{ij} \mid z_{ij}) p(z_{ij}) = \left[1 - \Phi(f_j^{(0)}(\mathbf{x}_i)) \right]^{z_{ij}} \Phi(f_j^{(0)}(\mathbf{x}_i))^{z_{ij}}$$

$$\begin{aligned}
& \times \left[\frac{\varphi(w_{ij}; f_j^{(0)}(\mathbf{x}_i), 1)}{1 - \Phi(f_j^{(0)}(\mathbf{x}_i))} \right]^{1-z_{ij}} \left[\frac{\varphi(w_{ij}; f_j^{(0)}(\mathbf{x}_i), 1)}{\Phi(f_j^{(0)}(\mathbf{x}_i))} \right]^{1-z_{ij}} \\
& = \varphi(w_{ij}; f_j^{(0)}(\mathbf{x}_i), 1).
\end{aligned}$$

where $\varphi(x; \mu, \sigma^2)$ denotes the density of the Gaussian distribution with mean μ and variance σ^2 . Using the above result for all categories $j \in \{1, \dots, d\}$ and observations $i \in \{1, \dots, n\}$ in conjunction with (6), we obtain the desired expression in (7).

S.2.2 Posterior inference

Following the notation defined in Section 2.6, we here present the computations of the integrated likelihood functions of the trees and the full conditional distributions of their corresponding terminal node parameters, which are given in (9) and (10) for the compositional probabilities $f_j^{(c)}$ and in (11) and (12) for the structural zero probabilities $f_j^{(0)}$, respectively.

Following Murray (2021), let $f_{(h)j}^{(c)}(\mathbf{x}_i) = \prod_{\ell \neq h} g(\mathbf{x}_i; \mathcal{T}_{\ell j}^{(c)}, \Lambda_{\ell j}^{(c)})$. From the augmented likelihood function of the ZANIM-LN-BART model given in (7), the conditional likelihood function for $(\mathcal{T}_{hj}^{(c)}, \Lambda_{hj})$ can be derived as follows

$$\begin{aligned}
\mathcal{L}(\mathcal{T}_{hj}^{(c)}, \Lambda_{hj} \mid \mathcal{T}_{(h)j}^{(c)}, \Lambda_{(h)j}, \dots) & \propto \prod_{i=1}^n \left[f_j^{(c)}(\mathbf{x}_i) \right]^{y_{ij}} \exp \left\{ -\phi_i z_{ij} e^{u_{ij}} f_j^{(c)}(\mathbf{x}_i) \right\} \\
& \propto \prod_{i=1}^n \left[f_{(h)j}^{(c)}(\mathbf{x}_i) g(\mathbf{x}_i; \mathcal{T}_{hj}^{(c)}, \Lambda_h^{(c)}) \right]^{y_{ij}} \\
& \quad \times \exp \left\{ -\phi_i z_{ij} e^{u_{ij}} f_{(h)j}^{(c)}(\mathbf{x}_i) g(\mathbf{x}_i; \mathcal{T}_{hj}^{(c)}, \Lambda_h^{(c)}) \right\} \\
& \propto \prod_{t \in \mathcal{L}_{hj}^{(c)}} \prod_{i: \mathbf{x}_i \in \mathcal{A}_{htj}^{(c)}} \left[f_{(h)j}^{(c)}(\mathbf{x}_i) \lambda_{hjt} \right]^{y_{ij}} e^{-\phi_i z_{ij} e^{u_{ij}} f_{(h)j}^{(c)}(\mathbf{x}_i) \lambda_{hjt}} \\
& \propto \prod_{t \in \mathcal{L}_{hj}^{(c)}} \lambda_{hjt}^{r_{htj}^{(c)}} e^{-s_{htj}^{(c)} \lambda_{hjt}},
\end{aligned}$$

where $r_{htj}^{(c)} = \sum_{i: \mathbf{x}_i \in \mathcal{A}_{htj}^{(c)}} y_{ij}$ and $s_{htj}^{(c)} = \sum_{i: \mathbf{x}_i \in \mathcal{A}_{htj}^{(c)}} \phi_i z_{ij} e^{u_{ij}} f_{(h)j}^{(c)}(\mathbf{x}_i)$ play the role of sufficient statistics.

Using the above expression for the conditional distribution of $(\mathcal{T}_{hj}^{(c)}, \Lambda_{hj})$, and recalling the conditionally conjugate priors, $\lambda_{htj} \stackrel{\text{ind.}}{\sim} \text{Gamma}[c_0, d_0]$, we obtain the full conditional posterior density for the terminal node parameters as follows:

$$\pi(\Lambda_{(h)j} \mid \mathcal{T}_{hj}^{(c)}, \mathcal{T}_{(h)j}^{(c)}, \Lambda_{(h)j}, \dots) \propto \prod_{t \in \mathcal{L}_{hj}^{(c)}} \frac{d_0^{c_0}}{\Gamma(c_0)} \lambda_{hjt}^{r_{htj}^{(c)} + c_0 - 1} \exp \left\{ -(s_{htj}^{(c)} + d_0) \lambda_{hjt} \right\},$$

such that $(\lambda_{htj} \mid \cdot) \stackrel{\text{ind.}}{\sim} \text{Gamma}[r_{htj}^{(c)} + c_0, s_{htj}^{(c)} + d_0]$, as given in (10).

The branching process prior proposed by Chipman et al. (1998) for the tree topologies is given by

$$\pi_{\mathcal{T}}(\mathcal{T}_h) = \prod_{t \in \mathcal{B}_h} [a(1 + d_{ht})^{-b}] \prod_{t \in \mathcal{L}_h} [1 - a(1 + d_{ht})^{-b}],$$

where d_{ht} is the depth of node t in tree h and $a \in (0, 1)$ and $b \geq 0$ are hyperparameters, with recommended values of $a = 0.95$ and $b = 2$. Note that $a(1 + d_{ht})^{-b}$ gives the probability of node t of tree h being an internal node at depth d_{ht} . By considering this tree prior, we obtain the integrated likelihood of tree $\mathcal{T}_{hj}^{(c)}$ as follows:

$$\pi(\mathcal{T}_{hj}^{(c)} \mid \mathcal{T}_{(h)j}^{(c)}, \Lambda_{(h)j}, \dots) \propto \pi_{\mathcal{T}}(\mathcal{T}_{hj}^{(c)}) \int \prod_{t \in \mathcal{L}_{hj}^{(c)}} \frac{d_0^{c_0}}{\Gamma(c_0)} \lambda_{hjt}^{r_{htj}^{(c)} + c_0 - 1} \exp \left\{ -(s_{htj}^{(c)} + d_0) \lambda_{hjt} \right\} d\lambda_{hjt}$$

$$\propto \pi_{\mathcal{T}} \left(\mathcal{T}_{hj}^{(c)} \right) \prod_{t \in \mathcal{L}_{hj}^{(c)}} \frac{d_0^{c_0}}{\Gamma(c_0)} \frac{\Gamma \left(r_{htj}^{(c)} + c_0 \right)}{(s_{htj}^{(c)} + d_0)^{r_{htj}^{(c)} + c_0}}.$$

Regarding the structural zero probabilities $f_j^{(0)}$, the steps of the derivation are straightforward and similar to those presented by [Chipman et al. \(2010\)](#). Expressed in terms of the vector of partial residuals $\mathbf{r}_{(h)j} = (r_{(h)1j}, \dots, r_{(h)nj})$, the conditional likelihood function for $(\mathcal{T}_{hj}^{(0)}, \mathcal{M}_{hj})$ is given by

$$\begin{aligned} \mathcal{L} \left(\mathcal{T}_{hj}^{(0)}, \mathcal{M}_{hj}; \mathbf{r}_{(h)j} \right) &\propto \prod_{i=1}^n \exp \left\{ -0.5 \left[r_{(h)ij} - g \left(\mathbf{x}_i, \mathcal{T}_{hj}^{(0)}, \mathcal{M}_{hj} \right) \right]^2 \right\} \\ &\propto \prod_{t \in \mathcal{L}_{hj}^{(0)}} \prod_{i: \mathbf{x}_i \in \mathcal{A}_{htj}^{(0)}} \exp \left[-0.5 (r_{(h)ij} - \mu_{htj})^2 \right] \\ &\propto \prod_{t \in \mathcal{L}_{hj}^{(0)}} \exp \left[-0.5 (n_{htj} \mu_{htj}^2 - 2\mu_{htj} s_{htj}^{(0)}) \right], \end{aligned}$$

where $s_{htj}^{(0)} = \sum_{i: \mathbf{x}_i \in \mathcal{A}_{htj}^{(0)}} r_{(h)ij}$ and n_{htj} is the total number of observations in the partition $\mathcal{A}_{htj}^{(0)}$. The expressions in (11) and (12) follow from well-known calculations based on the conditional likelihood function for $(\mathcal{T}_{hj}^{(0)}, \mathcal{M}_{hj})$ given above, together with the conjugate normal prior assumed for the terminal node parameters, i.e., $\mu_{htj} \stackrel{\text{ind.}}{\sim} \text{Normal}[0, \sigma_\mu^2]$.

S.2.2.1 Full conditionals for the random effects and factor analysis hyperparameters

An additional step in the ZANIM-LN-BART model is to update the random effects \mathbf{u}_i . As discussed in the main paper and explicitly written in (S.13), we consider a sum-to-zero constraint on the random effects \mathbf{u}_i in order to ensure identifiability. This implies that we effectively sample from the $(d-1)$ dimensional vector \mathbf{v}_i and map back through the transformation $\mathbf{u}_i = \mathbf{B}\mathbf{v}_i$.

From (S.13), the full conditional distribution of \mathbf{v}_i is given by

$$\pi(\mathbf{v}_i | \mathbf{y}_i, \mathbf{z}_i, \mathbf{f}) \propto \prod_{j=1}^d \left(\frac{\exp \left\{ (\mathbf{B}\mathbf{v}_i)_j \right\}}{\sum_{k=1}^d z_{ik} f_k^{(c)}(\mathbf{x}_i) \exp \{ (\mathbf{B}\mathbf{v}_i)_k \}} \right)^{y_{ij}} \varphi(\mathbf{v}_i; \mathbf{0}_{d-1}, \boldsymbol{\Sigma}_V), \quad (\text{S.14})$$

where $\varphi(\mathbf{x}; \boldsymbol{\mu}, \boldsymbol{\Sigma})$ denotes the density of the d -dimensional multivariate normal distribution with mean $\boldsymbol{\mu}$ and covariance matrix $\boldsymbol{\Sigma}$. We sample from the above full conditional using the elliptical slice sampling algorithm ([Murray et al., 2010](#)).

As discussed in Section 2.5, we assume a factor-analytic hyperprior on \mathbf{v}_i via the decomposition:

$$\mathbf{v}_i = \boldsymbol{\Gamma}\boldsymbol{\eta}_i + \boldsymbol{\epsilon}_i,$$

where $\boldsymbol{\Gamma} = [\gamma_{jk}]_{j=1, \dots, d-1}^{k=1, \dots, q}$ is a $(d-1) \times q$ factor loading matrix, $\boldsymbol{\eta}_i \sim \text{Normal}_q[\mathbf{0}_q, \mathbf{I}_q]$, and $\boldsymbol{\epsilon}_i \sim \text{Normal}_{d-1}[\mathbf{0}_{d-1}, \boldsymbol{\Psi}]$, with $\boldsymbol{\Psi} = \text{diag}\{\psi_1, \dots, \psi_{d-1}\}$. We further include the shrinkage-inducing multiplicative gamma process prior (MGP) of [Bhattacharya and Dunson \(2011\)](#), which is defined as follows

$$\begin{aligned} (\gamma_{jk} | \rho_{jk}, \tau_k) &\sim \text{Normal} \left[0, \rho_{jk}^{-1} \tau_k^{-1} \right], \quad \rho_{jk} \sim \text{Gamma} [\nu/2, \nu/2], \quad \tau_k = \prod_{\ell=1}^k \varrho_\ell \\ \varrho_1 &\sim \text{Gamma} [a_1, 1], \quad \varrho_h \sim \text{Gamma} [a_2, 1], \quad h \geq 2, \quad \psi_j \sim \text{Gamma} [a_\psi, b_\psi], \end{aligned}$$

where τ_k is a global shrinkage parameter for the k -th column, and $[\rho_{jk}]_{j=1, \dots, d-1}^{k=1, \dots, q}$ are local shrinkage parameters for each corresponding element of $\boldsymbol{\Gamma}$.

Let $\mathbf{V} \in \mathbb{R}^{n \times d-1}$ be the matrix whose rows are denoted by $\{\mathbf{v}_i\}_{i=1}^n \in \mathbb{R}^{d-1}$ and let $\mathbf{v}^{(j)} \in \mathbb{R}^n$ denote the j -th column of \mathbf{V} . Similarly, let $\mathbf{H} \in \mathbb{R}^{n \times q}$ denote the factor score matrix with rows $\boldsymbol{\eta}_1, \dots, \boldsymbol{\eta}_n \in \mathbb{R}^q$. From

Bayesian linear regression results, the full conditional distribution of γ_j is

$$(\gamma_j | \mathbf{v}^{(j)}, \mathbf{H}) \sim \text{Normal}_q \left[(D_j^{-1} + \psi_j^{-1} \mathbf{H}^\top \mathbf{H})^{-1} \psi_j^{-1} \mathbf{H}^\top \mathbf{v}^{(j)}, (D_j^{-1} + \psi_j^{-1} \mathbf{H}^\top \mathbf{H})^{-1} \right]. \quad (\text{S.15})$$

where $D_j^{-1} = \text{diag}(\rho_{j1}\tau_1, \dots, \rho_{jq}\tau_q)$. From conditional results of the multivariate normal distribution, the full conditional distribution of η_i is

$$(\eta_i | \mathbf{v}_i, \mathbf{\Gamma}, \mathbf{\Psi}) \sim \text{Normal}_q \left[(\mathbf{I}_q + \mathbf{\Gamma}^\top \mathbf{\Psi}^{-1} \mathbf{\Gamma})^{-1} \mathbf{\Gamma} \mathbf{\Psi}^{-1} \mathbf{v}_i, (\mathbf{I}_q + \mathbf{\Gamma}^\top \mathbf{\Psi}^{-1} \mathbf{\Gamma})^{-1} \right]. \quad (\text{S.16})$$

As both (S.15) and (S.16) are multivariate normal distributions, we note that both updates can be performed efficiently by employing block updates (Rue and Held, 2005).

It is also easy to see that the full conditional distribution of ψ_j is

$$(\psi_j^{-1} | \mathbf{v}^{(j)}, \gamma_j, \mathbf{H}) \sim \text{Gamma} \left[n/2 + a_\psi, (\mathbf{v}^{(j)} - \mathbf{H}\gamma_j)^\top (\mathbf{v}^{(j)} - \mathbf{H}\gamma_j) / 2 + b_\psi \right]. \quad (\text{S.17})$$

Finally, the full conditional of the local shrinkage parameters ρ_{jk} is given by

$$(\rho_{jk} | \dots) \sim \text{Gamma} \left[\frac{\nu + 1}{2}, \frac{\nu + \tau_k \gamma_{jk}^2}{2} \right], \quad (\text{S.18})$$

for $j = 1 \dots, (d-1)$ rows and $k = 1, \dots, q$ columns. The full conditional distributions of the global shrinkage parameters $\tau_k = \prod_{\ell=1}^k \varrho_\ell$ are updated sequentially, after sampling from the full conditional distribution of ϱ_1 , given by

$$(\varrho_1 | \dots) \sim \text{Gamma} \left[a_1 + (d-1)q/2, 1 + 0.5 \sum_{\ell=1}^q \left(\tau_\ell^{(1)} \sum_{j=1}^{d-1} \rho_{j\ell} \gamma_{j\ell}^2 \right) \right], \quad (\text{S.19})$$

and, for $h \geq 2$, the full conditional distribution of ϱ_h given by

$$(\varrho_h | \dots) \sim \text{Gamma} \left[a_2 + (d-1)/2(q-h+1), 1 + 0.5 \sum_{\ell=h}^q \left(\tau_\ell^{(h)} \sum_{j=1}^{d-1} \rho_{j\ell} \gamma_{j\ell}^2 \right) \right], \quad (\text{S.20})$$

where $\tau_\ell^{(h)} = \varrho_h^{-1} \prod_{t=1}^h \varrho_t$.

S.2.3 Inferential algorithm

To present the algorithm, we denote the transition kernels of the tree proposals by $K(\mathcal{T}_h^{(c)}, \cdot)$ and $K(\mathcal{T}_h^{(0)}, \cdot)$. Our implementation uses the mixture of grow, prune, and change proposals introduced in Chipman et al. (1998). We refer to Kapelner and Bleich (2016) for further description of these transition kernels in the classical BART model of Chipman et al. (2010), which we adapt for the trees of our ZANIM-LN-BART model. Algorithm S.1 gives our implementation of the inference scheme for the ZANIM-LN-BART model in full.

S.3 Additional results for the simulation studies

In Section 3.2, we evaluated the performance of the ZANIM-BART, ZANIM-LN-BART and ZIDM-reg models under a misspecified data generating process, considering $d = 20$ categories, different sample sizes $n \in \{100, 500, 1000\}$, total counts N_i drawn from the discrete uniform on $[1000, 5000]$, and $p = 6$ covariates. For completeness, we report the traceplots of the KL divergences for the sample sizes $n = 100$ and $n = 1000$ in Fig. S.2 and Fig. S.3, respectively.

Algorithm S.1: MCMC algorithm to fit the ZANIM-LN-BART model.

Input: Data $\{\mathbf{y}_i, \mathbf{x}_i\}_{i=1}^n$, numbers of trees m_θ and m_ζ , number of iterations R , and all hyperparameters of the priors.

Initialise: The BART priors parameters associated with $f_j^{(c)}(\mathbf{x}_i)$ and $f_j^{(0)}(\mathbf{x}_i)$ for all $j \in \{1, \dots, d\}$ categories: $\{\mathcal{T}_{hj}^{(c)}, \Lambda_{hj}\}_{h=1}^{m_\theta}$ and $\{\mathcal{T}_{hj}^{(0)}, \mathcal{M}_{hj}\}_{h=1}^{m_\zeta}$, respectively. The tree topologies are initialised as stumps and the terminal node parameters are set to $\lambda_{h1j} = 1.0$ and $\mu_{h1j} = 0.0$. Draw from the priors of z_{ij} and \mathbf{v}_i and set $\mathbf{u}_i = \mathbf{Bv}_i$.

1 **for** iterations t from 1 to R **do**

2 Update $(\phi_i \mid \mathbf{y}_i, \mathbf{z}_i, \mathbf{u}_i, \mathbf{f}^{(c)}(\mathbf{x}_i))$ from its full conditional in (5).

3 **for** categories j from 1 to d **do**

4 Update $(z_{ij} \mid y_{ij}, u_{ij}, \phi_i, f_j^{(c)}, f_j^{(0)})$ from its full conditional in (8).

5 Update $w_{ij} \sim \text{TN}_{[-\infty, 0]}[f_0^{(j)}(\mathbf{x}_i), 1]$ if $z_{ij} = 1$ and $\text{TN}_{[0, \infty]}[f_0^{(j)}(\mathbf{x}_i), 1]$ if $z_{ij} = 0$, $\forall i \in \{1, \dots, n\}$.

6 **for** trees h from 1 to m_θ **do**

7 Sample $\mathcal{T}' \sim K(\cdot \mid \mathcal{T}_{hj}^{(c)})$.

8 Compute the acceptance probability using the integrated likelihood in (9) as follows:

$$\alpha(\mathcal{T}_{hj}^{(c)}, \mathcal{T}') = 1 \wedge \frac{\pi(\mathcal{T}' \mid \mathcal{T}_{(h)j}^{(c)}, \Lambda_{(h)j}, \dots) K(\mathcal{T}_{hj}^{(c)} \mid \mathcal{T}')}{\pi(\mathcal{T}_{hj}^{(c)} \mid \mathcal{T}_{(h)j}^{(c)}, \Lambda_{(h)j}, \dots) K(\mathcal{T}' \mid \mathcal{T}_{hj}^{(c)})}.$$

9 Set $\mathcal{T}_{hj}^{(c)} = \mathcal{T}'$ with probability $\alpha(\mathcal{T}_{hj}^{(c)}, \mathcal{T}')$.

10 Sample from the full conditionals of the terminal node parameters Λ_{hj} in (10).

11 **end**

12 **for** trees h from 1 to m_ζ **do**

13 Sample $\mathcal{T}' \sim K(\cdot \mid \mathcal{T}_{hj}^{(0)})$.

14 Compute the acceptance probability using the integrated likelihood in (11) as follows:

$$\alpha(\mathcal{T}_{hj}^{(0)}, \mathcal{T}') = 1 \wedge \frac{\pi(\mathcal{T}' \mid \mathcal{T}_{(h)j}^{(0)}, \mathcal{M}_{(h)j}, \dots) K(\mathcal{T}_{hj}^{(0)} \mid \mathcal{T}')}{\pi(\mathcal{T}_{hj}^{(0)} \mid \mathcal{T}_{(h)j}^{(0)}, \mathcal{M}_{(h)j}, \dots) K(\mathcal{T}' \mid \mathcal{T}_{hj}^{(0)})}.$$

15 Set $\mathcal{T}_{hj}^{(0)} = \mathcal{T}'$ with probability $\alpha(\mathcal{T}_{hj}^{(0)}, \mathcal{T}')$.

16 Sample from the full conditionals of the terminal node parameters \mathcal{M}_{hj} in (10).

17 **end**

18 Update \mathbf{v}_i from its full conditional in (S.14) using elliptical slice sampling, and then set $\mathbf{u}_i = \mathbf{Bv}_i$.

19 Update the factor analysis hyperparameters $\boldsymbol{\gamma}_i$, $\boldsymbol{\eta}_i$, and $\boldsymbol{\psi}_j$ from their full conditional distributions in (S.15), (S.16), and (S.17), respectively.

20 Update the shrinkage-inducing MGP hyperparameters ρ_{jk} , ϱ_1 , and ϱ_h , $h \geq 2$ from their respective full conditional distributions in (S.18), (S.19), and (S.20), along with τ_k .

21 **end**

22 **end**

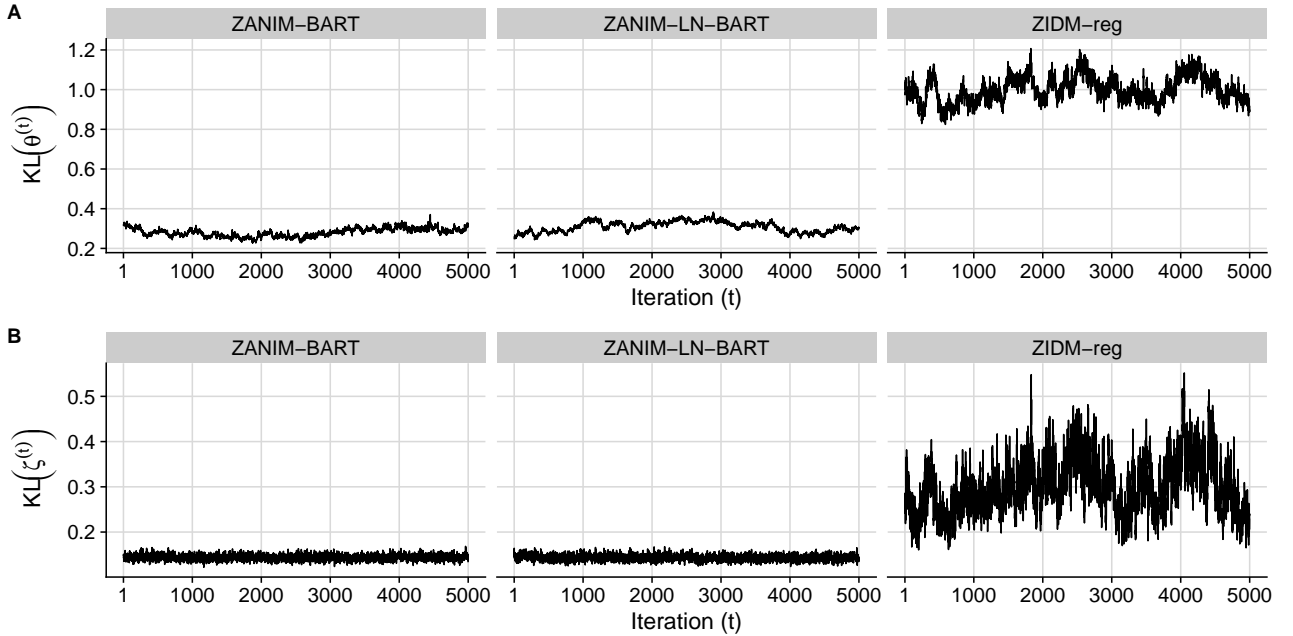


Fig. S.2: Traceplots of $KL(\theta^{(t)})$ in Panel **A** and $KL(\zeta^{(t)})$ in Panel **B** under the ZANIM-BART, ZANIM-LN-BART, and ZIDM-reg models for a sample size of $n = 100$.

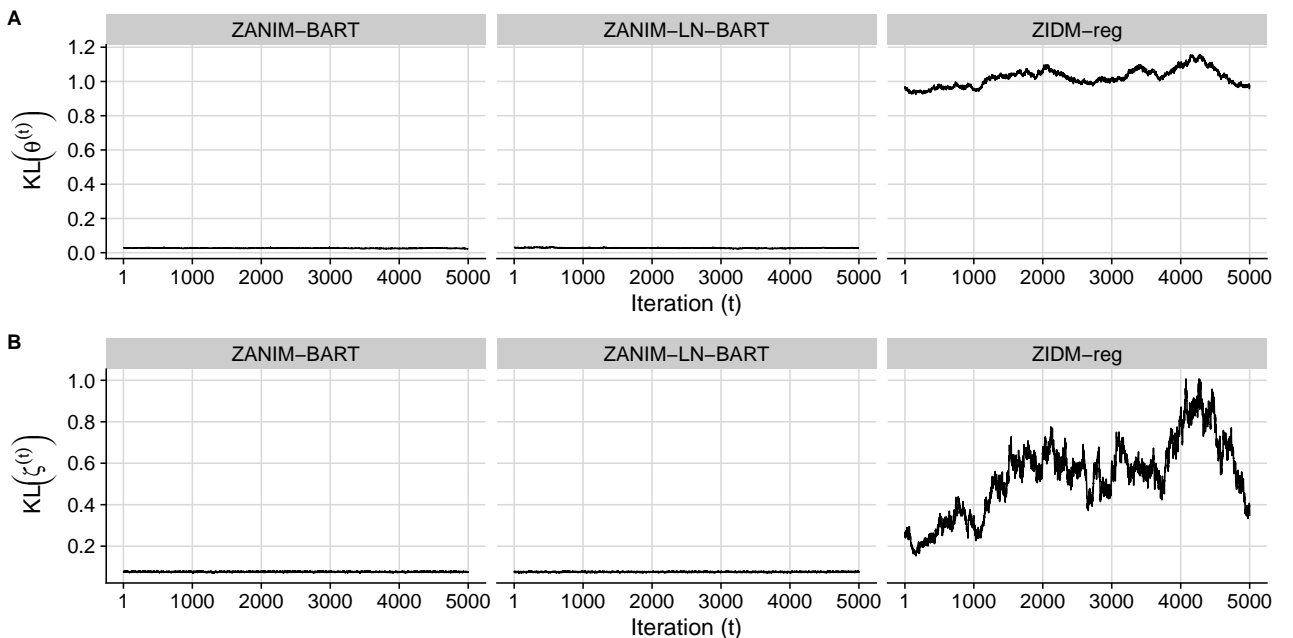


Fig. S.3: Traceplots of $KL(\theta^{(t)})$ in Panel **A** and $KL(\zeta^{(t)})$ in Panel **B** under the ZANIM-BART, ZANIM-LN-BART, and ZIDM-reg models for a sample size of $n = 1000$.

S.4 Additional results for the microbiome data analyses

Regarding the analyses of the benchmark human gut microbiome data set presented in Section 4.1, we now assess the MCMC convergence of the ZANIM-LN-BART, ZANIM-BART, ZIDM-reg, and DM-reg models applied to these data by computing the Frobenius norm between the empirical compositions, y_{ij}/N_i , and the corresponding model-based predictions given by the posterior draws of the individual-level count-probabilities,

$\vartheta_{ij}^{(t)}$, across the iterations $t \in \{1, \dots, R\}$. This quantity is defined by

$$\text{FROB}(\vartheta^{(t)}) = \sqrt{\sum_{i=1}^n \sum_{j=1}^d \left(y_{ij}/N_i - \vartheta_{ij}^{(t)} \right)^2}, \quad t \in \{1, \dots, R\}. \quad (\text{S.21})$$

Convergence assessments for the standard BART model of [Chipman et al. \(2010\)](#) typically rely on monitoring the residual standard deviation parameter. As there is no such parameter available under our ZANIM-BART and ZANIM-LN-BART models, we follow the approach discussed by [Sparapani et al. \(2021\)](#) for other BART-based models and adapt traditional MCMC diagnostics to our case using the estimator $\text{FROB}(\vartheta^{(t)})$ defined in [\(S.21\)](#). This quantity is also available and of interest for the ZIDM-reg and DM-reg models, thereby facilitating a fair comparison. Indeed, [Koslovsky \(2023\)](#) averaged this quantity as a measure of goodness-of-fit of the ZIDM-reg model, albeit without monitoring its trace as we do in [Fig. S.4](#), which shows the traceplots of $\text{FROB}(\vartheta^{(t)})$ under all four models. The results suggest that the models achieve good mixing and that their predicted compositions are consistent with the empirical compositions y_{ij}/N_i .

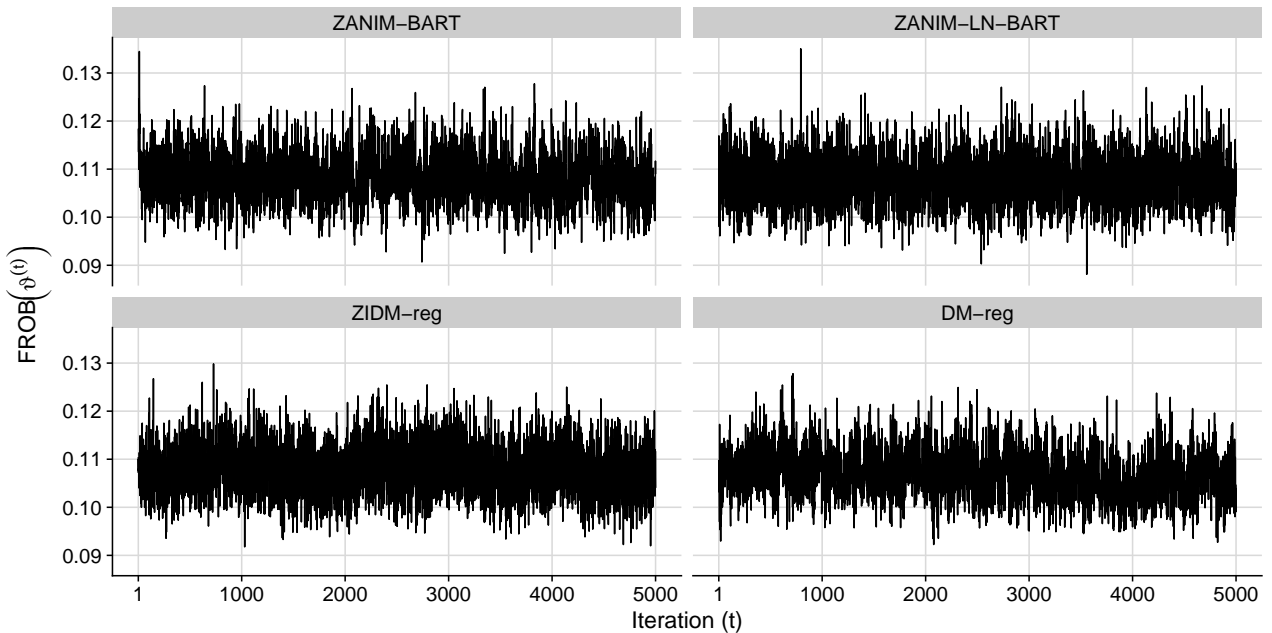


Fig. S.4: Traceplots of the Frobenius norm defined in [\(S.21\)](#) between the empirical compositions, y_{ij}/N_i , and the corresponding model-based predictions given by the posterior draws $\vartheta_{ij}^{(t)}$ for the ZANIM-BART, ZANIM-LN-BART, ZIDM-reg, and DM-reg models. The corresponding effective sample sizes are 1051.56, 2144.05, 635.50, and 460.59.

In [Fig. 4](#), we compare the marginal ECDF of the relative abundances, y_{ij}/N_i , with the corresponding posterior predictive distributions under the four models for the *Bacteroides* and *Prevotella* taxa. To summarise the goodness-of-fit of the models, we compute the average rank probability score (RPS; [Murphy, 1970](#)) based on the ECDF and the corresponding posterior predictive distributions of the relative abundances under all four models for all $d = 28$ taxa. The results given in [Table S.2](#) show that, overall, the ZANIM-LN-BART model provides the best fit to the data, with the lowest values of RPS for 22 out of the 28 taxa.

We now illustrate a particularly useful characteristic of our proposed models: their ability to capture nonlinear dietary covariate effects in the microbiome data. Under the ZANIM-LN-BART model, we use the posterior projection method of [Woody et al. \(2021\)](#) to construct summaries of the posterior distribution of the compositional and structural zero probabilities $f_j^{(c)}(\mathbf{x}_i)$ and $f_j^{(0)}(\mathbf{x}_i)$, respectively. For each posterior sample of $f_j^{(c)}(\mathbf{x}_i)$, an optimal summary $\tilde{f}_j^{(c)}(\mathbf{x}_i)$ is calculated, considering a given class of summary functions \mathcal{Q} , via $\tilde{f}_j^{(c)}(\mathbf{x}_i) = \arg \min_{\kappa \in \mathcal{Q}} \|f_j^{(c)} - \kappa\|_2$. In our illustrations, we specify \mathcal{Q} as the family of generalised additive models. The specific choice of basis expansion is not central; indeed, [Woody et al. \(2021\)](#) argue that any

Table S.2: Values of the average rank probability score (RPS, lower is better), scaled by 100 and computed from the marginal empirical cumulative distribution of each taxa and the corresponding posterior predictive distribution under the ZANIM-BART, ZANIM-LN-BART, ZIDM-reg, and DM-reg models. The lowest values are indicated in bold.

Taxa	ZANIM-BART	ZANIM-LN-BART	ZIDM-reg	DM-reg
<i>Actinomycineae</i>	0.008	0.006	0.039	0.046
<i>Alistipes</i>	0.963	0.631	2.570	2.884
<i>Anaerotruncus</i>	0.015	0.014	0.076	0.074
<i>Anaerovorax</i>	0.026	0.017	0.120	0.111
<i>Bacteroides</i>	2.731	2.579	8.660	13.278
<i>Bryantella</i>	0.009	0.010	0.021	0.042
<i>Clostridiaceae</i>	0.030	0.021	0.086	0.116
<i>Coprobacillus</i>	0.058	0.042	0.066	0.097
<i>Coprococcus</i>	0.023	0.020	0.062	0.064
<i>Coriobacterineae</i>	0.028	0.021	0.084	0.088
<i>Dialister</i>	0.431	0.300	0.723	0.823
<i>Dorea</i>	0.103	0.088	0.405	0.376
<i>Erysipelotrichaceae</i>	0.123	0.088	0.404	0.411
<i>Faecalibacterium</i>	0.656	0.595	1.751	1.933
<i>Holdemania</i>	0.019	0.014	0.077	0.077
<i>Lachnospira</i>	0.051	0.052	0.101	0.112
<i>Lachnospiraceae</i>	0.975	0.837	2.625	3.220
<i>Parabacteroides</i>	0.509	0.487	2.225	2.527
<i>Peptostreptococcaceae</i>	0.144	0.080	0.456	0.443
<i>Prevotella</i>	3.217	3.281	2.701	9.620
<i>Roseburia</i>	0.267	0.244	1.207	1.323
<i>Ruminococcaceae</i>	0.077	0.086	0.692	0.707
<i>Ruminococcus</i>	0.370	0.287	0.649	0.724
<i>Streptococcus</i>	0.019	0.016	0.107	0.100
<i>Subdoligranulum</i>	0.316	0.303	1.239	1.310
<i>Sutterella</i>	0.398	0.479	0.411	0.669
<i>Turicibacter</i>	0.011	0.012	0.039	0.054
<i>Veillonella</i>	0.017	0.016	0.058	0.061

reasonable basis would be suitable. Our implementation uses the default settings of the `gam` function from the `mgcv` package in R (Wood, 2017). To measure the quality of the summary, Woody et al. (2021) recommended the use of the *summary R*², defined by

$$\text{summary } R^2 = 1 - \frac{\sum_{i=1}^n \left[f_j^{(c)}(\mathbf{x}_i) - \tilde{f}_j^{(c)}(\mathbf{x}_i) \right]^2}{\sum_{i=1}^n \left[f_j^{(c)}(\mathbf{x}_i) - \bar{f}_j^{(c)} \right]^2},$$

where $\bar{f}_j^{(c)} = n^{-1} \sum_{i=1}^n f_j^{(c)}(\mathbf{x}_i)$. Values of the summary R^2 closer to 1 indicate that the projected posterior distribution is a good approximation of $f_j^{(c)}(\mathbf{x}_i)$ at the observed values of the covariates. A similar procedure is performed for summarising $f_j^{(0)}(\mathbf{x}_i)$.

In our illustration, we focus on the *Prevotella* taxon, for which 67% of its observed counts are zero. For this taxon, the ZANIM-LN-BART model identifies 19 covariates associated with the compositional probabilities, θ_{ij} , with MPPI greater than 0.98. For the structural zero probabilities, ζ_{ij} , only the ‘Choline Sphingomyelin’ covariate has MPPI greater than 0.98. The results of the posterior projection for the compositional probabilities using three of the 19 identified covariates are given in Fig. S.5. From Panel **A**, we can see that the abundance of *Prevotella* in the human gut is affected by the levels of Potassium, Retinol, and Sodium through an exponential, sigmoidal, and otherwise nonlinear effect, respectively. The density plots in Panel **B** show the posterior distributions of the summary R^2 statistic, comparing the model with all dietary covariates against models obtained by omitting each one of the three predictors. Notably, omitting any of these covariates from the summary models leads to a substantial reduction in R^2 , consistent with the high MPPI of these covariates.

Finally, Fig. S.6 shows the effect of the only dietary covariate (Choline Sphingomyelin) with MPPI greater than 0.98 with respect to the structural zero probabilities. The projected posterior exhibits a nonlinear effect on the structural zero probabilities. Although the credible intervals are generally wide, reflecting uncertainty in the estimates, they narrow around values of Choline Sphingomyelin near zero, indicating an increase in the probability of a structural zero in this region of the covariate space. As before, omitting this covariate leads to a reduction in the summary R^2 statistic.

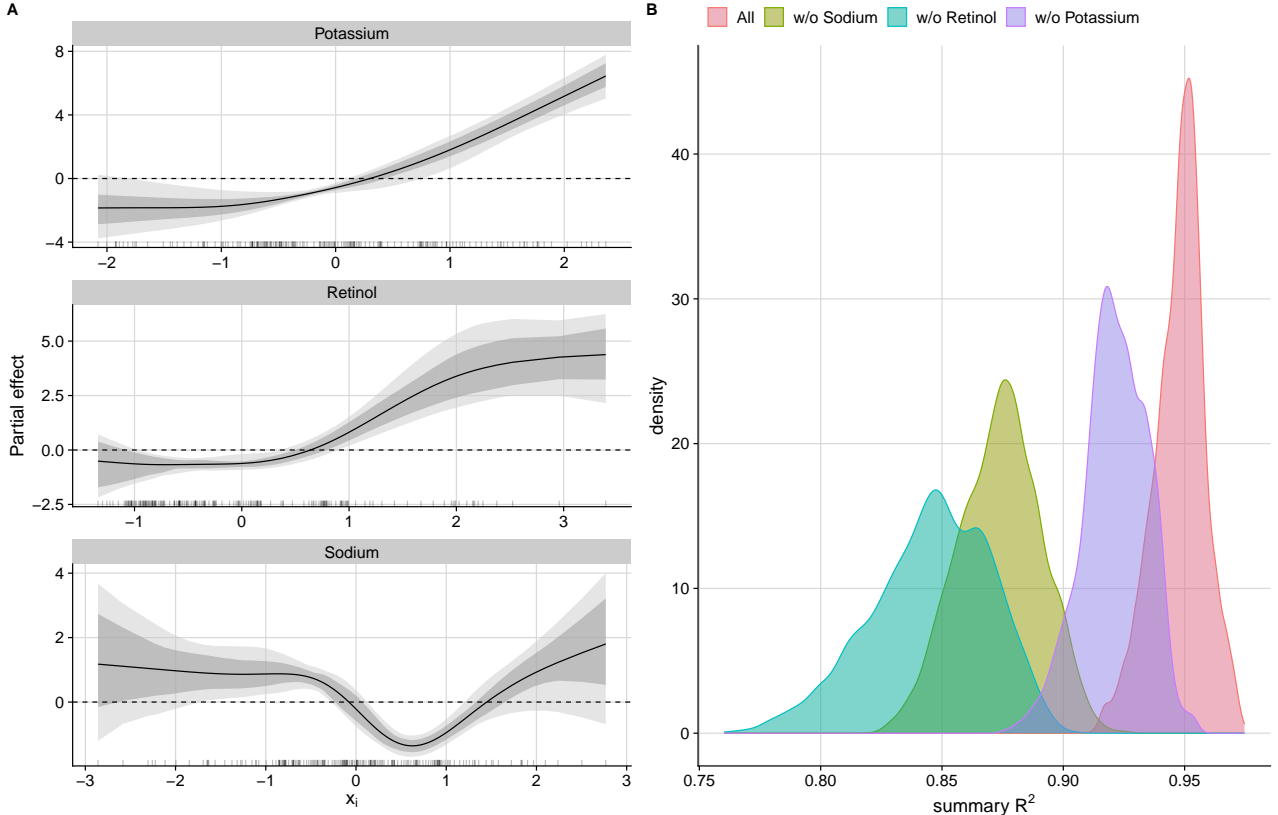


Fig. S.5: Posterior partial-effects summaries for the compositional probabilities (Panel A) and the corresponding summary R^2 measures (Panel B) under the ZANIM-LN-BART model for the *Prevotella* taxon across three dietary covariates with MPPI greater than 0.98. Solid black lines correspond to projected mean partial effects, with dark and light shaded grey areas representing 50% and 80% credible bands, respectively. Panel B shows the effects on the summary measure of incorporating all covariates and omitting each covariate one-by-one.

S.5 Additional results for the modern pollen-climate data analyses

Table S.3 gives taxa-specific descriptive statistics for the pollen-climate data analysed in Section 4.2, along with relative differences between the out-of-sample average RPS values under ZANIM-BART and ZANIM-LN-BART models, given by $\Delta \text{RPS} = (\text{RPS}_{\text{ZANIM-BART}} - \text{RPS}_{\text{ZANIM-LN-BART}}) / \text{RPS}_{\text{ZANIM-BART}}$. In addition, we report the average count, the percentage of zeros, the empirical dispersion index, $\text{DI}[Y_j]$, and the empirical version of the zero-inflation index, $\text{ZI}_b[Y_j]$, proposed by Blasco-Moreno et al. (2019) and used previously in Section S.1.

We can see from Table S.3 that all taxa present high levels of overdispersion and 16 of the 28 taxa have $\text{ZI}_b > 0$ indicating zero-inflation that cannot be explained solely by modelling taxa-specific variations. Hence, explicit modelling of the zero-inflation, as per our ZANIM-BART and ZANIM-LN-BART models, can be a suitable alternative for explaining the excess of zeros. We note that relative differences between the out-of-sample average RPS values under the ZANIM-BART and ZANIM-LN-BART models are positive for all taxa except *Ulmus*, indicating that ZANIM-LN-BART yields lower RPS values and thus provides a better description of the data than ZANIM-BART.

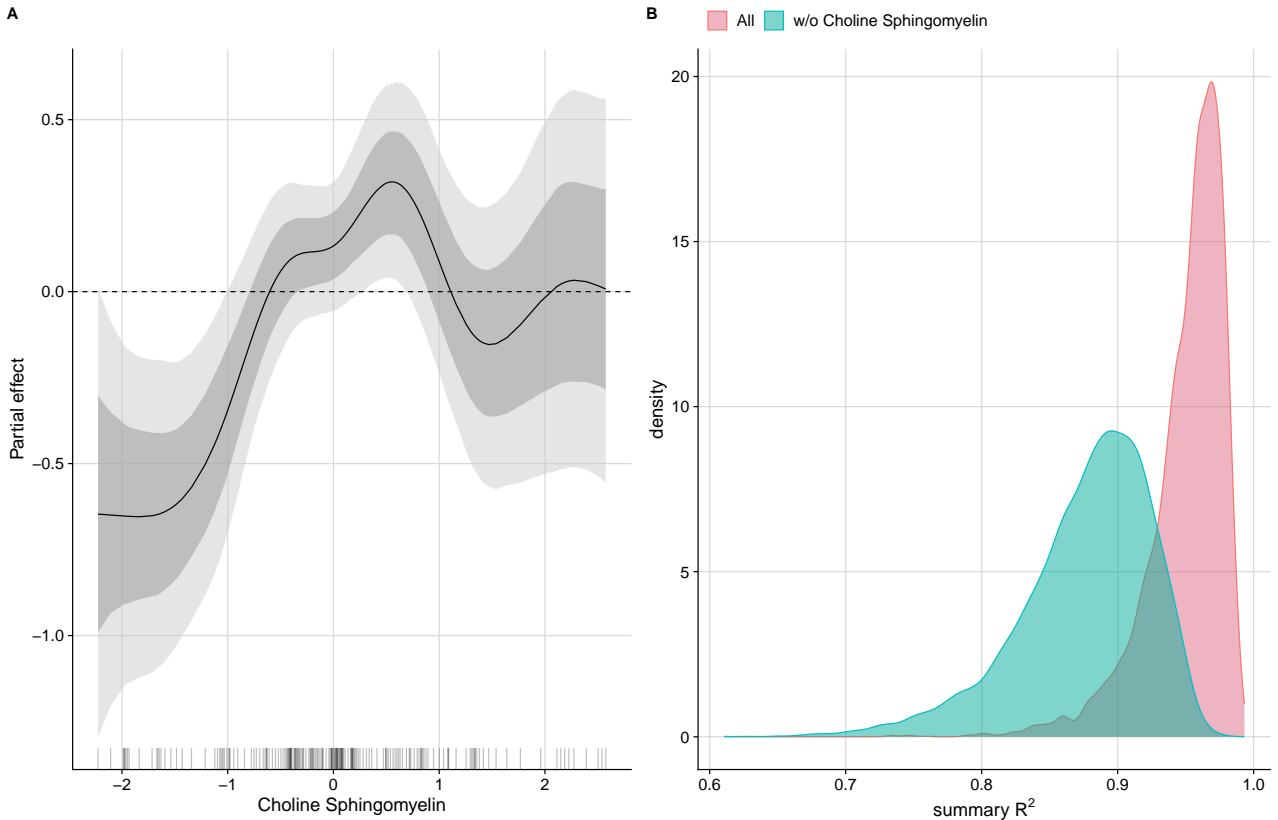


Fig. S.6: Posterior partial effects summaries for the population-level zero-inflation probability (Panel **A**) and the corresponding summary R^2 measures (Panel **B**) under the ZANIM-LN-BART model for the *Prevotella* taxon for the only dietary covariate (Choline Sphingomyelin) with MPPI greater than 0.98. Solid black lines denote projected mean partial effects, with dark and light shaded grey areas representing 50% and 80% credible bands, respectively. Panel **B** shows the effects on the summary measure of incorporating all covariates and omitting each covariate one-by-one.

Fig. 7 in the main paper shows the partial dependence plots (PDPs) for the *Picea* and *Pinus.D* taxa with the marginal effects of the MTCO, GDD5, and AET/PET covariates. We now provide complementary PDPs for all $d = 28$ taxa in Fig. S.7, Fig. S.8, and Fig. S.9, with the effects of MTCO, GDD5, and AET/PET, respectively, on the compositional (blue curves) and structural zero (orange curves) probabilities.

Fig. S.10 shows the empirical correlations of the counts, the posterior mean correlations of the random effects of the ZANIM-LN-BART model, and the means of the posterior-predictive correlations of the counts under the ZANIM-BART and ZANIM-LN-BART models. We can see that the posterior-predictive correlation matrix under ZANIM-LN-BART aligns with the empirical one, while the ZANIM-BART model fails to capture some important dependencies. This is consistent with the better overall performance of the ZANIM-LN-BART model in describing the modern-pollen data. Moreover, this figure highlights how the latent correlations under ZANIM-LN-BART model can uncover dependence patterns that are not detected by the raw correlations of the counts, providing insights into potential dependencies among the taxa. For instance, the empirical correlation matrix suggests that *Ephedra* shows little similarity with any other taxa. In contrast, the posterior mean of the latent correlation matrix reveals moderate negative and positive associations between *Ephedra* and several other taxa.

Table S.3: Descriptive statistics of the $d = 28$ taxa for the modern pollen-climate data, along with relative differences between the out-of-sample average RPS values under ZANIM-BART and ZANIM-LN-BART models, i.e., $\Delta \text{RPS} = (\text{RPS}_{\text{ZANIM-BART}} - \text{RPS}_{\text{ZANIM-LN-BART}}) / \text{RPS}_{\text{ZANIM-BART}}$. The RPS values were computed using the marginal ECDF of the relative abundances, y_{ij}/N_i , and the corresponding posterior predictive distribution obtained from 2000 held-out samples.

Taxa	Average count	% zeros	$\text{DI}[Y_j]$	$\text{ZI}_b[Y_j]$	ΔRPS
<i>Abies</i>	10.81	66.16	122.88	0.03	0.21
<i>Alnus</i>	69.92	20.51	196.69	0.16	0.15
<i>Artemisia</i>	38.35	37.79	309.33	-0.36	0.18
<i>Betula</i>	140.03	25.11	193.07	0.64	0.10
<i>Carpinus</i>	2.27	91.06	141.59	-0.17	0.14
<i>Castanea</i>	1.72	92.71	309.46	-1.37	0.23
<i>Cedrus</i>	3.03	96.65	470.18	0.14	0.22
<i>Chenopodiaceae</i>	39.33	37.90	321.46	-0.37	0.18
<i>Corylus</i>	7.31	78.69	125.16	0.16	0.09
<i>Cyperaceae</i>	51.24	26.16	220.80	-0.07	0.20
<i>Ephedra</i>	1.15	94.11	161.94	-0.68	0.05
<i>Ericales</i>	14.90	71.82	206.28	0.14	0.29
<i>Fagus</i>	13.21	70.93	162.83	0.17	0.15
<i>Gramineae</i>	103.08	10.27	198.62	0.18	0.14
<i>Juniperus</i>	17.51	59.82	258.97	-0.36	0.18
<i>Larix</i>	1.60	93.25	144.21	-0.26	0.15
<i>Olea</i>	10.28	84.98	194.72	0.42	0.19
<i>Ostrya</i>	4.68	73.94	41.15	0.30	0.06
<i>Phillyrea</i>	1.12	93.12	96.80	-0.34	0.29
<i>Picea</i>	87.09	37.37	256.58	0.48	0.09
<i>Pinus.D</i>	225.28	6.66	210.42	0.53	0.09
<i>Pinus.H</i>	4.80	97.11	402.60	0.59	0.01
<i>Pistacia</i>	2.02	91.41	193.75	-0.63	0.26
<i>Quercus.D</i>	77.80	40.04	265.59	0.44	0.05
<i>Quercus.E</i>	19.77	85.71	403.79	0.48	0.29
<i>Salix</i>	18.10	41.47	219.01	-0.97	0.15
<i>Tilia</i>	1.54	85.16	79.42	-0.87	0.17
<i>Ulmus</i>	9.52	60.20	57.46	0.26	-0.01

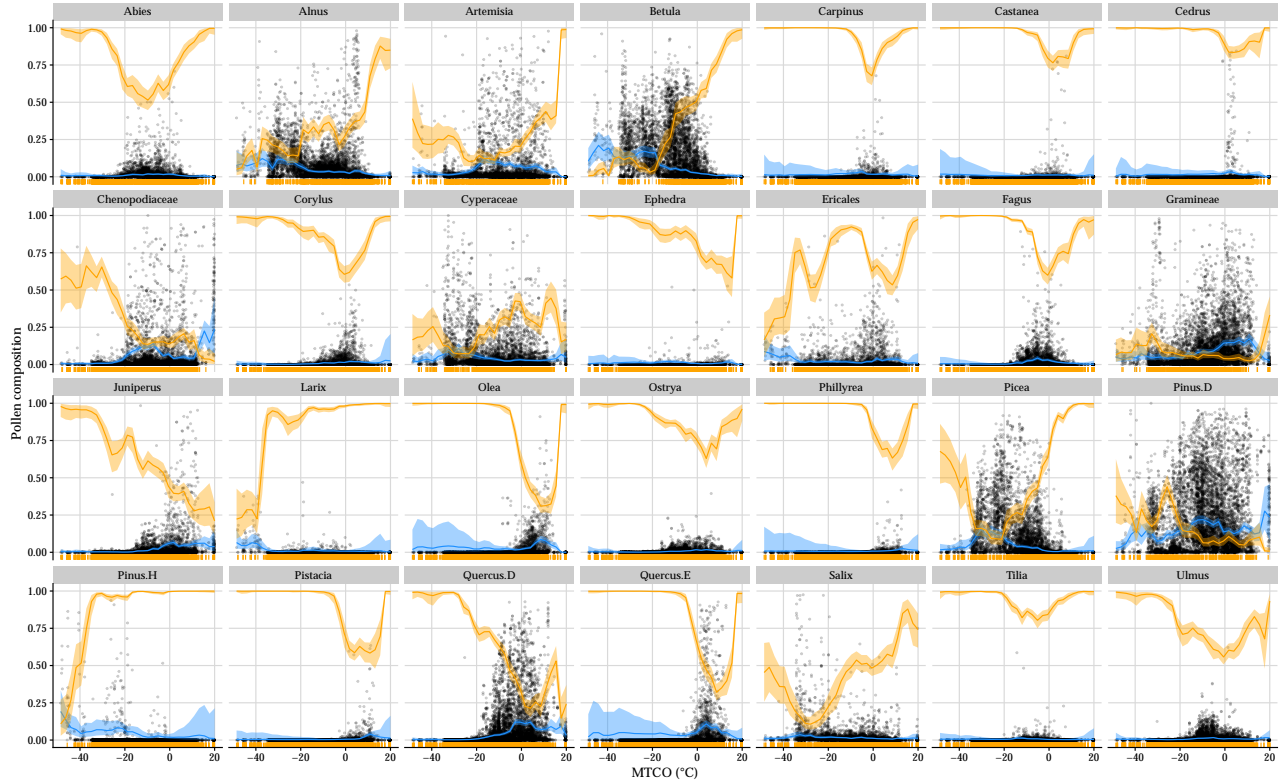


Fig. S.7: Partial dependence plots, with associated 95% credible interval bands, for all $d = 28$ pollen taxa, showing the effects of the MTCO covariate on both the compositional (blue) and structural zero (orange) probabilities under the ZANIM-LN-BART model. Black dots represent the observed relative abundances, y_{ij}/N_i , and the orange rugs along the x -axes represent samples where the observed counts are zero.

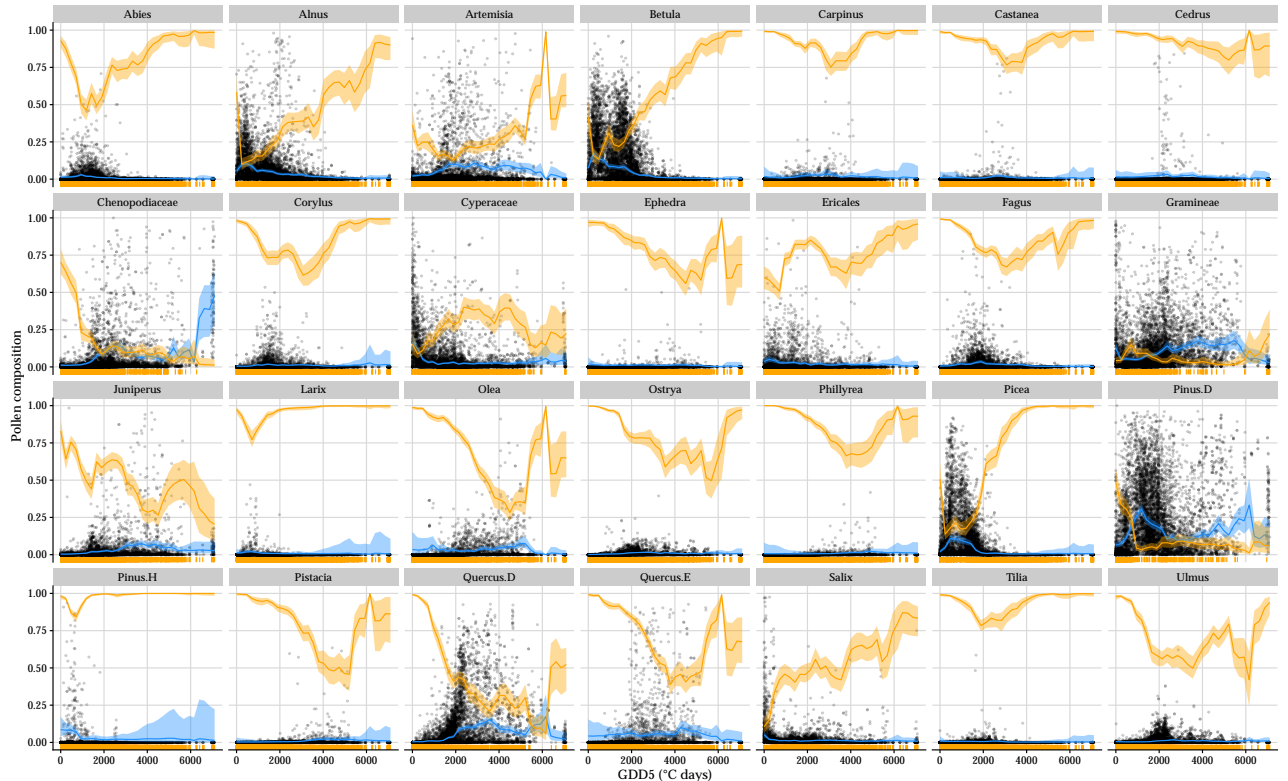


Fig. S.8: Partial dependence plots, with associated 95% credible interval bands, for all $d = 28$ pollen taxa, showing the effects of the GDD5 covariate on both the compositional (blue) and structural zero (orange) probabilities under the ZANIM-LN-BART model. Black dots represent the observed relative abundances, y_{ij}/N_i , and the orange rugs along the x -axes represent samples where the observed counts are zero.

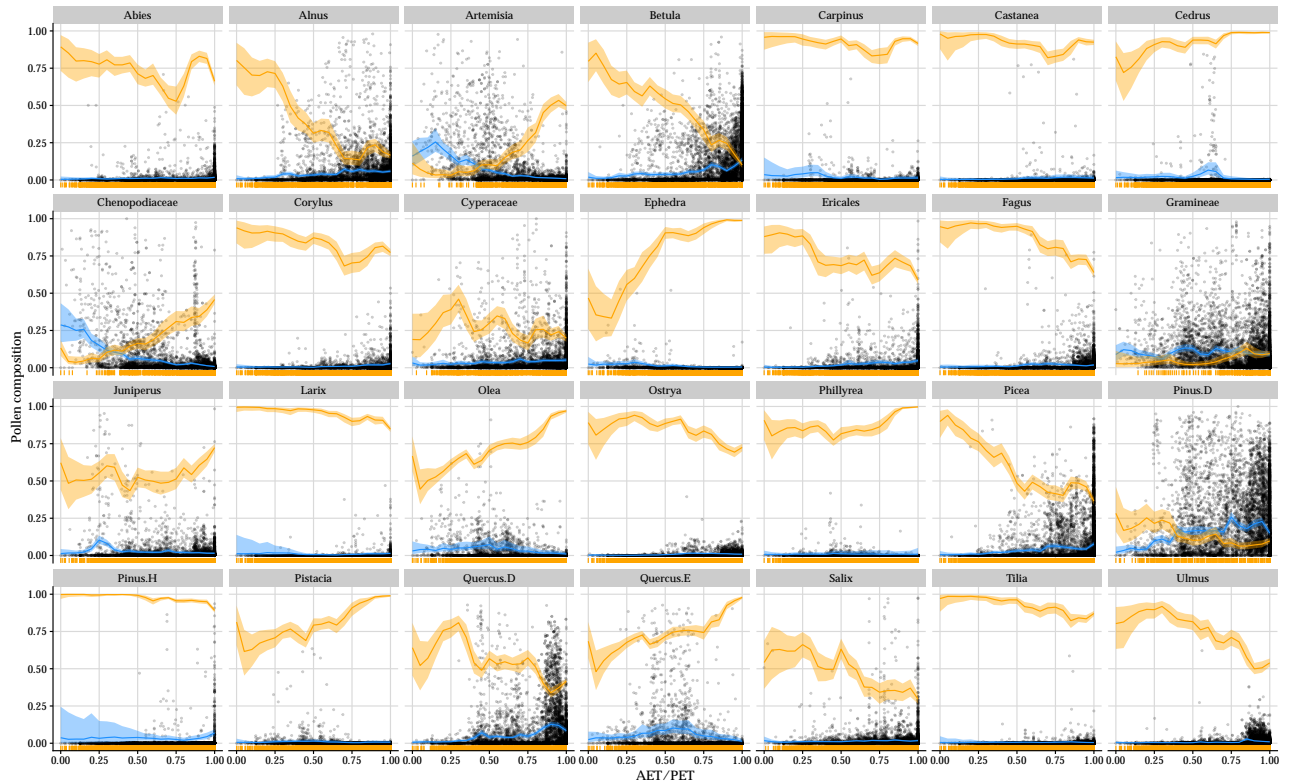


Fig. S.9: Partial dependence plots, with associated 95% credible interval bands, for all $d = 28$ pollen taxa, showing the effects of the AET/PET covariate on both the compositional (blue) and structural zero (orange) probabilities under the ZANIM-LN-BART model. Black dots represent the observed relative abundances, y_{ij}/N_i , and the orange rugs along the x -axes represent samples where the observed counts are zero.

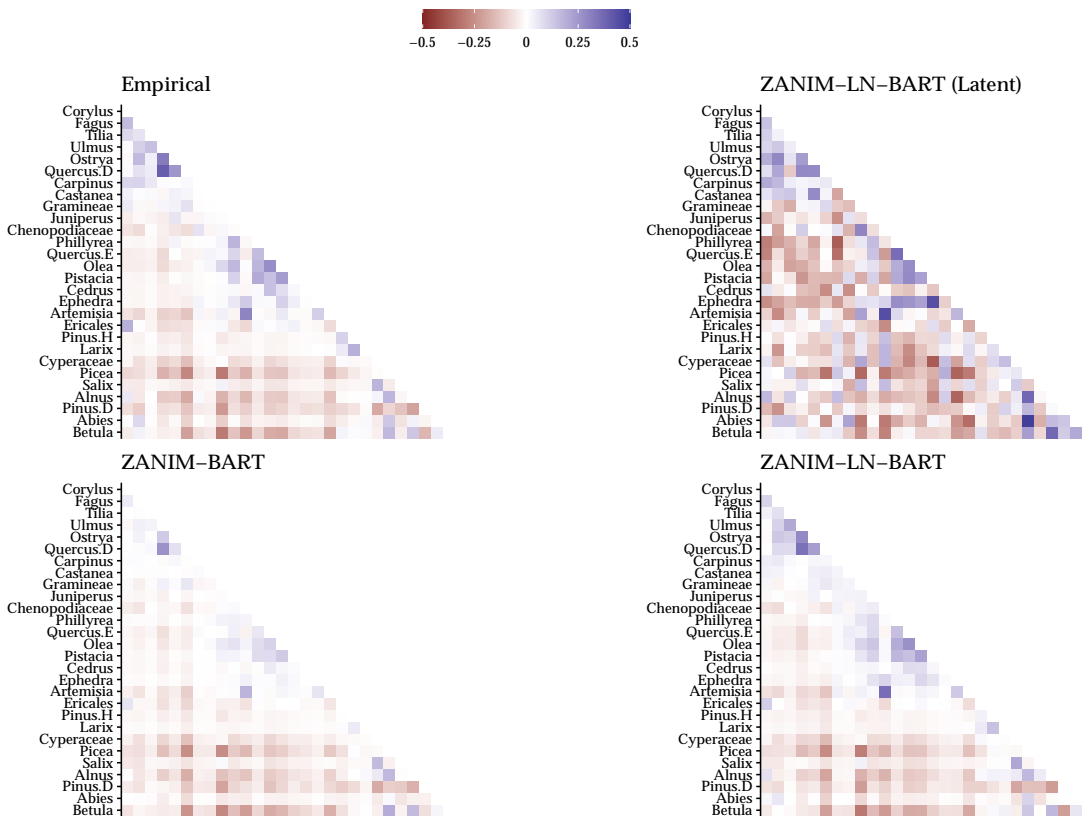


Fig. S.10: Empirical correlations of the counts (top left), posterior mean correlations of the latent random effects under the ZANIM-LN-BART model (top right), and the means of the posterior-predictive correlations of the counts under the ZANIM-BART (bottom left) and ZANIM-LN-BART (bottom right) models. Each row in the heat map corresponds to a taxon in each case.